The mitogen-activated protein kinase (MAPK) pathway is the major pathway transferring the *ras* signal, in which three different routes are known; the ERK, p38, and c-jun N-terminal kinase (JNK) pathways [15]. The activity of these MAP kinases was examined under standard or low serum conditions (Fig. 3D). The amount of phosphorylated ERK (pERK) was much greater in ihMSC-*ras* than in ihMSC under both standard and serum-free conditions (Fig. 3D). The amount of phosphorylated p38 (pp38) showed no significant difference between ihMSC and ihMSC-*ras* (Supplementary Fig. 3), and hardly any phosphorylated JNK was observed in any cell line (data not shown). Therefore, the expression of the oncogenic *ras* gene in ihMSC induced the phosphorylation of ERK in a serum-independent manner. U0126, a specific inhibitor for MEK, a kinase of ERK, was used to inhibit the ERK activity in the hMSC-*ras* lines. All three cell lines showed a reduction in the expression of pERK after the treatment with U0126 (Supplementary Fig. 4). The morphology of ihMSC and ihMSC-*ras* was compared before and after the treatment. ihMSC showed no remarkable morphological change after the treatment with U0126 (data not shown), whereas the number of ihMSC-*ras* cells with autophagosomes was significantly reduced (Fig. 3E) These results indicated the induction of autophagy by oncogenic H-ras$^{Val12}$.

### *Differentiation potential of ihMSC-ras*

#### *Adipogenic differentiation*

After the induction, ihMSC-*ras*-1 showed Oil-Red-O-positive droplets (Fig. 4A, a) as did ihMSC (Fig. 1E, a). In the case of ihMSC, the expression the PPARγ gene was silent in the non-induced state, and became positive after the adipogenic induction, whereas ihMSC-*ras* expressed the PPARγ gene without the induction in association with the AP2 gene, which was one of the genes downstream of the PPARγ gene (Fig. 4B). In contrast, the expression of the adipsin gene was not induced in ihMSC-*ras* (Fig. 4B).

#### *Osteogenic differentiation*

The osteogenic differentiation of ihMSC-*ras*-1 was significantly inhibited. ihMSC ras-1 formed almost no alizarin-red-positive calcified nodules (Fig. 4A, b), which were abundantly observed in ihMSC (Fig. 1E, b). As for the mRNA expression, the most striking difference between ihMSC-Mock-1 and ihMSC-*ras*-1 was in the gene expression of osteocalcin (OC) and its regulator, OSF2/RUNX2 (Fig. 4B). Under standard culture conditions, ihMSC-Mock-1 expressed the OSF2/RUNX2 gene weakly, which was evoked by the osteogenic induction (Fig. 4B). No expression of the OSF2/RUNX2 gene, however, was observed in ihMSC-*ras*-1 and the expression of the OC gene also remained suppressed (Fig. 4B).

#### *Chondrogenic differentiation*

After 3 weeks of chondrogenic induction, the ihMSC-*ras*-1 produced a solid pellet in the three-dimensional culture, which contained matrices positive for Alcian blue staining (Fig. 4A, c). The gene expression of cartilage oligomeric matrix protein (COMP), aggrecan (AGC), and to a lesser extent, α1 chain of type 2 collagen (COL2A1) was upregulated in hMSC-*ras* (Fig. 4B). These results suggested

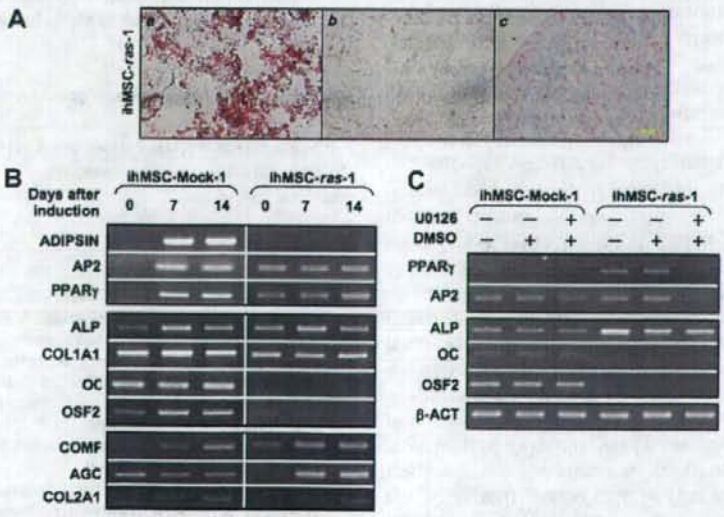


Fig. 4. Potential of ihMSC-*ras* to differentiate. (A) Lineage-related histochemical staining after the induction of each lineage. (B) mRNA expression of lineage-related genes after the induction of each lineage in ihMSC-Mock and ihMSC-*ras*. (C) mRNA expression of adipogenic and osteogenic lineage-related genes in ihMSC-Mock and ihMSC-*ras* with or without treatment with U0126.

that the oncogenic H-ras$^{Val12}$ protein had no significant effect on the chondrogenic differentiation.

The mRNA expression of adipo- and osteo-related genes in cells treated with U0126 was analyzed by RT-PCR (Fig. 4C). The expression of the PPARγ and AP2 genes in ihMSC-*ras* was reduced when the cells were treated with U0126 (Fig. 4C), whereas no restoration of the expression of the OSF2/RUNX2 and OC genes was observed (Fig. 4C). These results suggested that the acceleration of adipogenic differentiation was mediated through the ERK pathway, but the loss of osteogenic potential was caused by other pathways. Identical results were obtained in ihMSC-ras-2 (data not shown), suggesting the constant effect of H-ras$^{Val12}$ for the differentiation potential of ihMSC.

## Discussion

As far as we know, this is the first report of the transformation of hMSC *in vitro*. The result was compatible with a previous spontaneous transformation of hTERT-introduced hMSC, in which p16$^{INK4A}$ was inactivated by a deletion and the K-*ras* gene was mutated [16].

The transformation of ihMSC by the H-*ras*$^{Val12}$ gene revealed two interesting findings. First, the oncogenic H-*ras*$^{Val12}$ induced, to our surprise, autophagy in ihMSC. Autophagy is a critical process responsible for the degradation of intracellular material by a membrane of uncertain origin to form an autophagosome that sequesters such material and subsequently fuses with the lysosome [13], and involved in physiological processes as well as pathological conditions such as neurodegenerative disease, cardiomyopathies, and cancer [17]. Because autophagy is suppressed in most cancer cells, autophagy-related genes may work as tumor suppressors [18]. In some types of cancer cells, however, autophagy was activated as a defense mechanism to protect against poor nutrition in tumor tissues [18]. Therefore, it is not clear whether the autophagy observed in ihMSC-*ras* reflected the process of transformation or not. However, because this feature was constantly observed in two independently established cell lines, it might be used as a morphological feature to detect potentially transformed cells *in vitro*. The relationship between the *ras* signal and autophagy is controversial. Raf-1 is an effector for MAPK signaling pathways, which constitute three routes; ERK, p38, and JNK [19]. Activation of raf-1 induced autophagy in colon cancer HT-29 cells through the activation of ERK [19], indicating that the *ras* signal stimulates autophagy. On the other hand, the introduction of the H-*ras*$^{Val12}$ gene into NIH3T3 reduced the autophagy stimulated by nutrient starvation through the activation of class I PI3-K [20]. Thus the PI3-K pathway and MAPK pathway exert opposite effects on autophagy, and the effect of the activation of ras may depend on cell specificity. We have shown that the introduction of H-*ras*$^{Val12}$ into ihMSC induced autophagy through the activation of the ERK pathway without growth inhibition.

Second, the H-*ras*$^{Val12}$-mediated transformation completely abolished the osteogenic potential of ihMSC. OSF2, an osteoblast-specific form of the RUNX2 transcription factor, is shown to play a central role in determining osteogenic and adipogenic differentiation. OSF2/RUNX2−/− chondrocytes differentiate spontaneously *in vitro* into adipogenic cells expressing the PPARγ gene, and introduction of the OSF2/RUNX2 gene inhibited the expression of the PPARγ gene [21]. On the other hand, PPARγ activated by its ligand inhibited the DNA-binding activity of OSF2/RUNX2, and therefore the gene expression of its targets such as OC [22]. In this report, activated *ras* induced the expression of the PPARγ gene and accelerated the adipogenic differentiation, which mimicked the effect of knocking out OSF2/RUNX2. However, inhibition of the ERK pathway by U0126 inhibited the expression of PPARγ without restoring the expression of the OSF2/RUNX2 gene, suggesting that the induction of PPARγ expression by H-*ras*$^{Val12}$ was independent of the inactivation of OSF2/RUNX2. Because activated mutations of *ras* genes are rarely found in osteosarcomas [23], there must be molecules fulfilling the role of the ras signal in osteosarcomas. The ihMSC described here can serve as a material to investigate the oncogenic properties and effects on differentiation of candidate molecules.

## Acknowledgments

This work was supported by Grants-in-aid for Scientific Research from the Japan Society for the Promotion of Science, and from the New Energy and Industrial Technology Development Organization. The authors thank Dr. Noboru Mizushima for allowing them to use the anti-LC3 antibody, Drs. Soichi Adachi, and Motonobu Watanabe for helpful advice.

## Appendix A. Supplementary data

Supplementary data associated with this article can be found, in the online version, at doi:10.1016/j.bbrc.2006.11.137.

## References

[1] T. Aoyama, T. Okamoto, S. Nagayama, K. Nishijo, T. Ishibe, K. Yasura, T. Nakayama, T. Nakamura, J. Toguchida, Methylation in the core-promoter region of the chondromodulin-I gene determines the cell-specific expression by regulating the binding of transcriptional activator Sp3, J. Biol. Chem. 279 (2004) 28789–28797.

[2] M.F. Pittenger, A.M. Mackay, S.C. Beck, R.K. Jaiswal, R. Douglas, J.D. Mosca, M.A. Moorman, D.W. Simonetti, S. Craig, D.R. Marshak, Multilineage potential of adult human mesenchymal stem cells, Science 284 (1999) 143–147.

[3] M. van Lohuizen, S. Verbeek, B. Scheljen, E. Wientjens, H. van der Guiden, A. Berns, Identification of cooperating oncogenes in Eμ-myc transgenic mice by provirus tagging, Cell 65 (1991) 737–752.

[4] J.J. Jacobs, B. Scheijen, J.W. Voncken, K. Kieboom, A. Berns, M. van Lohuizen, Bmi-1 collaborates with c-myc in tumorigenesis by

inhibiting c-myc-induced apoptosis via ink4a/ARF, Genes Dev. 13 (1999) 2678–2690.
[5] A.V. Molofsky, R. Pardal, T. Iwashita, I.K. Park, M.F. Clarke, S.J. Morrison, Bmi-1 dependence distinguishes neural stem cell self-renewal from progenitor proliferation, Nature 425 (2003) 962–967.
[6] K. Itahana, Y. Zou, Y. Itahana, J.L. Martinez, C. Beausejour, J.J. Jacobs, M. van Lohuizen, V. Band, J. Campisi, G.P. Dimri, Control of the replicative life span of human fibroblasts by p16 and the polycomb protein bmi-1, Mol. Cell. Biol. 23 (2003) 389–401.
[7] T. Maeda, H. Tashiro, M. Begum, H. Ohtake, T. Kiyono, H. Okamura, Establishment of an immortalized human ovarian surface epithelial cell line without chromosomal instability, Br. J. Cancer. 93 (2005) 116–123.
[8] Y. Takeda, T. Mori, H. Imabayashi, T. Kiyono, S. Gojo, S. Miyoshi, N. Hida, M. Ita, K. Segawa, S. Ogawa, M. Sakamoto, S. Nakamura, A. Umezawa, Can the life span of human marrow stromal cells be prolonged by bmi-1, E6, E7, and/or telomerase without affecting cardiomyogenic differentiation? J. Gene. Med. 6 (2004) 833–845.
[9] Y. Kabeya, N. Mizushima, T. Ueno, A. Yamamoto, T. Kirisako, T. Noda, E. Kominami, Y. Ohsumi, T. Yoshimori, LC3, a mammalian homologue of yeast Apg8p, is localized in autophagosome membranes after processing, EMBO J. 19 (2000) 5720–5728.
[10] T. Kiyono, S.A. Foster, J.I. Koop, J.K. McDougall, D.A. Galloway, A.J. Klingelhutz, Both Rb/p16$^{INK4a}$ inactivation and telomerase activity are required to immortalize human epithelial cells, Nature 396 (1998) 84–88.
[11] L.F. Parada, C.J. Tabin, C. Shih, R.A. Weinberg, Human EJ bladder carcinoma oncogene is homologue of Harvey sarcoma virus ras gene, Nature 297 (1982) 474–478.
[12] T. Okamoto, T. Aoyama, T. Nakayama, T. Nakamata, T. Hosaka, K. Nishijo, T. Nakamura, T. Kiyono, J. Toguchida, Clonal heterogeneity in differentiation potential of immortalized human mesenchymal stem cells, Biochem. Biophys. Res. Commun. 295 (2002) 354–361.
[13] W.A. Dunn Jr., Autophagy and related mechanisms of lysosome-mediated protein degradation, Trends Cell. Biol. 4 (1994) 139–143.
[14] I. Tanida, T. Ueno, E. Kominami, LC3 conjugation system in mammalian autophagy, Int. J. Biochem. Cell. Biol. 36 (2004) 2503–2518.
[15] T. Tanoue, E. Nishida, Molecular recognitions in the MAP kinase cascades, Cell. Signal. 15 (2003) 455–462.
[16] N. Serakinci, P. Guldberg, J.S. Burns, B. Abdallah, H. Schrodder, T. Jensen, M. Kassem, Adult human mesenchymal stem cell as a target for neoplastic transformation, Oncogene 23 (2004) 5095–5098.
[17] T. Shintani, D.J. Klionsky, Autophagy in health and disease: a double-edged sword, Science 306 (2004) 990–995.
[18] E. Ogier-Denis, P. Codogno, Autophagy: a barrier or an adaptive response to cancer, Biochim. Biophys. Acta 1603 (2003) 113–128.
[19] S. Pattingre, C. Bauvy, P. Codogno, Amino acids interfere with the ERK1/2-dependent control of macroautophagy by controlling the activation of Raf-1 in human colon cancer HT-29 cells, J. Biol. Chem. 278 (2003) 16667–16674.
[20] S. Furuta, E. Hidaka, A. Ogata, S. Yokota, T. Murata, Ras is involved in the negative control of autophagy through the class I PI3-kinase, Oncogene 23 (2004) 3898–3904.
[21] H. Enomoto, T. Furuichi, A. Zanma, K. Yamana, C. Yoshida, S. Sumitani, H. Yamamoto, M. Enomoto-Iwamoto, M. Iwamoto, T. Komori, Runx2 deficiency in chondrocytes causes adipogenic changes in vitro, J. Cell. Sci. 117 (2004) 417–425.
[22] B. Lecka-Czernik, I. Gubrij, E.J. Moerman, O. Kajkenova, D.A. Lipschitz, S.C. Manolagas, R.L. Jilka, Inhibition of Osf2/Cbfa1 expression and terminal osteoblast differentiation by PPARγ2, J. Cell. Biochem. 74 (1999) 357–371.
[23] F. Antillón-Klüssmann, M. García-Delgado, I. Villa-Elízag, L. Sierrasesúmaga, Mutational activation of ras genes is absent in pediatric osteosarcoma, Cancer Genet. Cytgenet. 79 (1995) 49–53.

STEM CELLS

TRANSLATIONAL AND CLINICAL RESEARCH: MESENCHYMAL STEM CELLS SERIES

# Expression of the p16INK4A Gene Is Associated Closely with Senescence of Human Mesenchymal Stem Cells and Is Potentially Silenced by DNA Methylation During In Vitro Expansion

KOTARO R. SHIBATA,[a,b] TOMOKI AOYAMA,[a] YASUKO SHIMA,[a,b] KENICHI FUKIAGE,[a] SEIJI OTSUKA,[a] MORITOSHI FURU,[a] YOSHIKI KOHNO,[a,b] KINYA ITO,[a] SHUNSUKE FUJIBAYASHI,[b] MASASHI NEO,[b] TOMITAKA NAKAYAMA,[b] TAKASHI NAKAMURA,[b] JUNYA TOGUCHIDA[a]

[a]Institute for Frontier Medical Sciences and [b]Graduate School of Medicine, Kyoto University, Kyoto, Japan

**Key Words.** Mesenchymal stem cells • Telomere • Methylation • p16INK4A • Senescence • BMI1

## ABSTRACT

**The precise biological characteristics of human mesenchymal stem cells (hMSCs), including growth regulatory mechanisms, have not yet been defined. Using 29 strains of hMSCs isolated from bone marrow, we have performed extensive analyses of the growth profiles of hMSCs in vitro. All 29 strains stopped proliferating with a mean population doubling (PD) of 28, although there was a considerable difference among strains. The mean telomere restriction fragment length of the cells passaged twice correlated well with the final number of PDs in each strain, suggesting the value of this measurement to be predictive of the growth potential of hMSCs. The expression level of the p16INK4A gene was associated closely with the PD number of each strain ($p = .00000001$). Most of the p16INK4A-positive cells were Ki67-negative and senescence associated β-galactosidase-positive, and the suppression of p16INK4A gene expression by small interfering RNA in senescent hMSCs reduced the number of senescent cells and endowed them with the ability to proliferate. Twenty-five of the 29 strains showed a steady gradual increase in the expression of p16INK4A. The remaining four strains (13.8%) showed different profiles, in which DNA methylation in the promoter region occurred in vitro. One of the four strains continued to proliferate for much longer than the others and showed chromosomal aberrations in the later stages. These results indicated p16INK4A to be a key factor in the regulation of hMSC growth, and, most importantly, careful monitoring of DNA methylation should be considered during the culture of hMSCs, particularly when a prolonged and extended propagation is required.** STEM CELLS *2007;25:2371–2382*

Disclosure of potential conflicts of interest is found at the end of this article.

## INTRODUCTION

Mesenchymal stem cells are defined as plastic-adherent fibroblastic cells with the potential to differentiate into multiple mesenchymal tissues. Human mesenchymal stem cells (hMSCs) isolated from bone marrow are able to proliferate in vitro and differentiate along multiple lineages including bone, cartilage, adipose, and muscle cells [1]. Thus, hMSCs are being tested in clinical trials for tissue regeneration and engineering [2, 3]. Although infinite growth ability is one definition of stem cells, most hMSCs cease proliferating after 20–40 population doublings (PDs) [4], although precisely why has not yet been elucidated. The proliferative capacity of primary mammalian cells in vitro is finite, a concept known as the Hayflick limit [5]. In vitro cultured cells undergo a limited number of PDs before entering a state of premature growth arrest, referred to as senescence, in which cells remain alive and metabolically active but are completely refractory to mitogenic stimuli [5]. As telomere shortening, oxidative stress, DNA damage, and aberrant mitogenic signaling can all induce senescence in human primary cells, senescence is now considered to be a form of biological protection from neoplastic transformation [6].

Telomeres, tandem TTAGGG repeats that cap the ends of eukaryotic chromosomes, are forced to shorten at each DNA replication. The shortening of telomeres plays an important role in cell aging and is regulated by a protein complex associated with telomere end [7, 8]. The maintenance of telomere ends is one of the mechanisms for self-renewal of stem cells. In undifferentiated hESCs, many proteins of the telomerase complex, including TERT, are expressed, and telomere length (8–11 kilobase [kb]) is maintained [9, 10]. In most characterized tissue stem cell subtypes such as hematopoietic stem cells (HSCs) and epidermal stem cells, telomeric shortening occurs with age despite the presence of telomerase activity [11].

Proteins regulating cell cycles are also involved in the cellular senescence process, among which $p16^{INK4A}$ has been studied extensively. $p16^{INK4A}$ was identified as a causative factor for familial melanomas and, simultaneously, as an inhibitor for the cell cycle kinases CDK4 and CDK6, indicating its properties as a tumor suppressor negatively regulating the cell cycle [12]. Subsequent investigations, however, have proved that the essential role of $p16^{INK4A}$ is actually in the regulation of cellular senescence. $p16^{INK4A}$ was found to be accumulated in many aged cells and tissues [13], and the age-induced increase in $p16^{INK4A}$ contributed to a reduction in the size of reservoirs of self-renewing tissue stem cells [14, 15]. The precise profile of $p16^{INK4A}$ gene expression during the in vitro culture of hMSCs has yet to be reported, and it is also unknown whether the

Correspondence: Tomoki Aoyama, M.D., Ph.D., Institute for Frontier Medical Sciences, Kyoto University, Kyoto, Japan. Telephone: +81-75-751-4107; Fax: +81-75-751-4646; e-mail: blue@frontier.kyoto-u.ac.jp Received March 28, 2007; accepted for publication June 5, 2007; first published online in STEM CELLS *EXPRESS* June 14, 2007. ©AlphaMed Press 1066-5099/2007/$30.00/0 doi: 10.1634/stemcells.2007-0225

shortening of telomere or the upregulation of $p16^{INK4A}$ expression is critical for senescence in hMSCs.

The activity of $p16^{INK4A}$ is regulated under both physiological and nonphysiological conditions. Under physiological conditions requiring the repression of $p16^{INK4A}$ such as in tissue stem cells, the transcription of the $p16^{INK4A}$ gene is downregulated by BMI1, a polycomb group (PcG) protein that affects stem cell fate, including self-renewal, senescence, and aging [16]. BMI1 is necessary for efficient self-renewing cell division in adult murine HSCs and neural stem cells (NSCs) [17, 18]. BMI1 represses the transcription of $p16^{INK4A}$ as well as $p14^{ARF}$, which is another inhibitor of cell proliferation sharing part of the coding sequence at the *INK4A-ARF* locus [19].

Under nonphysiological conditions such as in cancer cells, the most frequent event inactivating $p16^{INK4A}$ function is transcriptional downregulation by DNA methylation in the core promoter region [20]. In higher eukaryotes, DNA is methylated at cytosines located 5′ to guanosine in the CpG dinucleotide [21]. This modification has important regulatory effects on gene expression and also triggers de novo methylation in unmethylated lesions [22]. Therefore, the mapping of methylation patterns in CpG islands is an important tool for understanding both normal and pathologic gene expression events [23]. De novo methylation of the $p16^{INK4A}$ promoter regions in vitro was reported in spontaneously immortalized rodent cells, suggesting the important role of $p16^{INK4A}$ in bypassing the senescence. In this sense, it is interesting that the hMSCs transformed spontaneously in vitro lacked expression of the $p16^{INK4A}$ gene [24].

Here, we investigated the role of two critical factors, telomere length and the expression of $p16^{INK4A}$, during life span of hMSCs in vitro and found that both are involved in different phases. Also, we found that the prolonged propagation of hMSCs may induce inactivation of the $p16^{INK4A}$ gene by DNA methylation with chromosomal aberrations.

## Materials and Methods

### Study Population

Primary hMSCs were isolated from the bone marrow taken from iliac crests of 29 donors, who received orthopedic operative procedures requiring autologous bone grafts from iliac crests (supplemental online Table 1). The donors had no history of concurrent illness or of medication that could affect bone metabolism. There were 13 males and 16 females. The median donor age was 49.1 years (range, 10–84 years). The Ethics Committee of the Faculty of Medicine, Kyoto University, approved the procedure and informed consent was obtained from each donor.

### Cell Culture

Primary hMSC cultures were established by means of a previously described method [25]. Mononuclear cells were suspended in α-minimal essential medium with GlutaMAX (Invitrogen Co., Carlsbad, CA, http://www.invitrogen.com) supplemented with 10% fetal bovine serum (HyClone, South Logan, UT, http://www.hyclone.com), 100 U/ml penicillin, and 100 mg/ml streptomycin and seeded at a density of $2.5 \times 10^5$ cells per $cm^2$ in 5% $CO_2$ at 37°C. At 80% confluence, cells were counted and reseeded at a dilution of 1:3, as cells in the first passage. From this point, the number of PDs was calculated based on the total cell number at each passage. This procedure was repeated until the cells stopped proliferating. At this point, cell numbers were counted to calculate the final PD.

### Induction of Differentiation

The potential for differentiation in the osteogenic, adipogenic, and chondrogenic directions was examined using the differentiation-induction protocol provided by Cambrex (East Rutherford, NJ, http://www.cambrex.com) in each hMSC strain at the second passage. After 14 days of osteogenic differentiation, the cells were stained with 40 mM PH4.2 Alizarin Red S (Sigma-Aldrich, St. Louis, MO, http://www.sigmaaldrich.com). After 21 days of adipogenic differentiation, cells were stained with 0.3% oil red O (Nacalai Tesque, Kyoto, Japan, http://www.nacalai.co.jp/en/index.html). After 21 days of chondrogenic differentiation, the pellets were stained with Alcian Blue (Muto Pure Chemicals Co., LTD, Tokyo, http://www.mutokagaku.com).

### Telomere Length Assay

High molecular weight DNA was extracted from each hMSC at the second and final passage. Telomere restriction fragment length (TRFL) was determined using Southern blot analysis. Genomic DNA (2 μg) was digested by mixing HinfI and RsaI. The digested DNA was separated on 0.7% agarose gels. Gels were denatured and blotted onto a positively charged nylon membrane (Roche Diagnostics, Basel, Switzerland, http://www.roche-applied-science.com). Using the DIG Assay Kit (Roche Diagnostics), hybridization with a digoxigenin (DIG)-labeled telomere-specific probe (CCCTAA)3 was conducted. After hybridization, membranes were washed and incubated with a DIG-specific antibody covalently coupled to alkaline phosphatase (AP). Results were visualized using AP metabolizing chemiluminescent substrate (CSPD; Roche Diagnostics). Each assay was performed twice. Membranes were then scanned and the mean TRFL (mTRFL) was calculated.

### Western Blot Analysis

Western blotting was performed as mentioned [26]. The primary antibodies used were as follows: DO-1 for p53; G175-405 for $p16^{INK4A}$ (BD Pharmingen, San Diego, http://www.bdbiosciences.com), F-5 for $p21^{CIP1}$, C-19 for p27 (Santa Cruz Biotechnology, Santa Cruz, CA, http://www.scbt.com), and clone F6 for BMI1 (Upstate, Lake Placid, NY, http://www.upstate.com). Blots were probed with horseradish peroxidase-conjugated goat anti-mouse IgG or goat anti-rabbit IgG (Santa Cruz Biotechnology) and visualized using a chemiluminescence reagent ECL Plus Detection Kit (GE Healthcare UK Ltd, Little Chalfont, U.K., http://www.gehealthcare.com).

### Reverse Transcription-Polymerase Chain Reaction

Total RNA was extracted using TRIzol reagent (Invitrogen) and 1 μg was reverse transcribed for single-stranded cDNAs using oligo(dT) primer and Superscript II reverse transcriptase (Invitrogen).

### Quantitative Reverse Transcription-Polymerase Chain Reaction

The reaction mixtures for amplification contained 100 ng of cDNA and Universal TaqMan 2X Master Mix (Applied Biosystems, Foster City, CA, http://www.appliedbiosystems.com). The concentrations of primers and TaqMan probes (Biosearch Technologies Japan, Tokyo, http://www.btjkk.co.jp) were 900 and 250 nM. All reactions were performed in triplicate using the ABI PRISM 7700 Sequence Detection System (Applied Biosystems) under the following conditions: 2 minutes at 50°C and 10 minutes at 95°C followed by 40 cycles of 95°C for 15 seconds and 60°C for 1 minute. Expression of 18S was used as an internal control. Saos2, a human osteosarcoma cell line, expresses the $p16^{INK4A}$ gene at a high level due to a homozygous deletion of the retinoblastoma gene [27], and by setting the expression level of $p16^{INK4A}$ in Saos2 cells as a standard, the relative expression level of $p16^{INK4A}$ in hMSCs was calculated. A statistical analysis was done with the *t* test after logarithmic transformation. Primers and probes for $p16^{INK4a}$ are as described: sense, 5′-CCCAACGCACCGAATAGTTAC-3′; antisense, 5′-CACGGGTCGGGTGAGAGT-3′; probe, FAM-AGGCCGATCCAGGTCATGATGATGG-BHQ-1.

### Methylation-Specific Polymerase Chain Reaction

The bisulfite modification of DNA samples was performed using the EpiTect Bisulfite Kit (Qiagen, Tokyo, http://www1.qiagen.com). Methylation-specific polymerase chain reaction (PCR) (MSP)

for $p16^{INK4a}$ was performed as previously described [20, 28]. The methylation-specific primer sequences are as follows: sense, 5′-TTATTAGAGGGTGGGGCGGATCGC-3′; antisense, 5′-CAACCCCAAACCACAAC CATAA-3′. For the unmethylated region, the primers are: sense, 5′-TTATTAGAGGGTGGGGTGGATTGT-3′; antisense, 5′-CCACCTAAATCGACCTCCGACCG-3′.

### Small Interfering RNA Assay

The optimum sequence for the small interfering (si)RNA targeting the $p16^{INK4A}$ gene was obtained as ready-annealed, purified duplexes from Dharmacon Research (Lafayette, CO, http://www.dharmacon.com). The control "scrambled" sequence was AAGCGCGCUUUGUAGGAUUCG; the $p16^{INK4A}$-targeted sequence was AAACCAGAGGCAGUAACCAUG. Transfection was carried out using the Amaxa electroporation system (Amaxa Biosystems, Cologne, MA, http://www.amaxa.com).

### 5-Bromo-2′-deoxyuridine Assay

Incorporated 5-bromo-2′-deoxyuridine (BrdU) was detected with a BrdU Detection Kit (Roche Diagnostics) according to the manufacturer's instructions. Experiments were done in triplicate.

### Senescence Associated-β-Galactosidase Assay

Cells were cultured on eight-well chamber slides. The senescence associated-β-galactosidase (SA-β-Gal) assay was performed as described previously [29].

### Immunocytochemistry

After SA-β-Gal staining, cells were washed with phosphate-buffered saline (PBS) and permeabilized with 0.5% Triton X-100, 1% bovine serum albumin in PBS. Slides were blocked with 10% nonfat milk in PBS, incubated with primary antibody for 16 hours and with secondary antibody for 1 hour in blocking solution, counterstained with 4,6-diamidino-2-phenylindole, and viewed by epifluorescence microscopy. The antibodies used were DCS-50.2, a mouse monoclonal antibody for $p16^{INK4a}$ (Progen, Heidelberg, Germany, http://www.progen.de), and ab27619, a fluorescein isothiocyanate-conjugated rabbit monoclonal antibody for Ki-67 (Abcam, Cambridge, U.K., http://www.abcam.com).

### Statistical Analyses

Statistical analyses were performed using Statcel software. Data were assessed using the Pearson product-moment correlation coefficient, Student's *t* test, Spearman's rank-correlation coefficient analysis, a one-factor analysis of variance, a multiple regression analysis, and the Mantel-Haenszel chi-squared test.

## RESULTS

### Long-Term Culture of Human MSCs

The primary culture of donor cells was successful in all 29 cases, and the adipogenic, chondrogenic, and osteogenic differentiation of early passage cells was confirmed in all strains (supplemental online Fig. 1). Growth profiles of hMSCs showed characteristics typical of the Hayflick model of cellular aging (Fig. 1A), and all strains stopped proliferating after a certain period in vitro, although the culture period (mean, 151.2 ± 47.7 days; range, 90–334 days) and the final PD number (mean, 28.1 ± 7.2; range, 13–54) differed considerably among strains (supplemental online Table 1). There was a significant correlation between the final PD number and the age of donors ($p$ = .0042) with the Pearson product-moment correlation coefficient analysis. When each donor was classified by age into either a younger group (under 50 years, $n$ = 13, mean, 28.5 ± 12.2 years) (Fig. 1B) or an older group (over 50 years, $n$ = 16, mean, 66.6 ± 8.8 years) (Fig. 1C), the mean final PD number of the older group (24.8 ± 4.7) was found to be significantly less than that of the younger group (32.5 ± 7.5) ($p$ = .0086) (Fig. 1D). This result was confirmed by an analysis with Spearman's rank-correlation coefficient ($r$ = −.608, $p$ = .00128) (Fig. 1E).

### Telomere Length

Most of the cells at the final passage were flattened and enlarged (Fig. 2Ab), compatible with cells entering senescence. The flattened cells were positive for SA-β-gal staining (Fig. 2Ac) but negative for the terminal deoxynucleotidyl transferase dUTP nick-end labeling staining (data not shown), suggesting that the senescence was why the proliferation ceased. It is well known that the length of telomeres contributes to cellular senescence [30], and therefore the mTRFL was determined in each hMSC strain at the second and final passage, designated as SP and FP, respectively (Fig. 2B) (supplemental online Table 1). The mTRFL of SP and FP cells was 9.4 ± 1.0 kb and 7.5 ± 0.6 kb, respectively, and the mean telomere-shortening rate was 109 ± 43 base pairs (bp) (Fig. 2B). A Pearson product-moment correlation coefficient analysis showed a positive correlation ($p$ = .00048) between the mTRFL of SP and final PD. This result was confirmed with Spearman's rank-correlation coefficient ($r$ = −.557, $p$ = .00321) (Fig. 2C). These findings suggested that calculating the mTRFL of SP roughly predicts the expandability of the hMSC strain, which will be valuable information in expanding hMSC populations for clinical purposes. We then analyzed the correlation between the mTRFL of SP and donor age, but results of a Student's *t* test ($p$ = .13) (Fig. 2D) and Spearman's rank-correlation coefficient analysis ($r$ = −.28, $p$ = .13) (Fig. 2E) indicated that there was no correlation.

### PD Number-Dependent Increase of $p16^{INK4A}$ Gene Expression

The mTRFL of FP cells was 7.5 ± 0.6 kb, which is much longer than the critical size of the telomere (approximately 4.5 kb) [31], suggesting the involvement of other factors in the senescence of hMSCs. $p16^{INK4A}$, a cell cycle regulator, is known to contribute to cellular senescence and also stem cell aging [13]. The mRNA expression of the $p16^{INK4A}$ gene was analyzed in all hMSC strains at several time points. In most cases, the expression level of the $p16^{INK4A}$ gene showed a gradual increase during propagation in vitro (Fig. 3A). Using the expression level of Saos2 as a reference, the expression level of the p16 gene at each point was digitalized by quantitative reverse transcription (RT)-PCR and plotted against PD number (Fig. 3B). The PD-dependent increase in $p16^{INK4A}$ gene expression was confirmed statistically by a multiple regression analysis ($r$ = .78, $p$ = .00000056). A tight association was observed in both younger (Fig. 3B, circle) and older (Fig. 3B, triangle) donors.

The result of RT-PCR was confirmed by Western blotting. Seven cases were randomly selected, and proteins were extracted from cells at four time points based on the final PD number of each strain: the second passage (early); the PD number that is one third of the final PD number (early middle); the PD number that is two thirds of the final PD number (late middle); and the last passage (final). The expression of $p16^{INK4A}$ protein at each point was analyzed as well as that of $p21^{cip1}$, p27, and p53 and quantified. As in the case of mRNA expression, the expression level of $p16^{INK4A}$ protein showed a PD-dependent increase ($p$ = .000000001). As for the other cell cycle regulating genes, the $p21^{cip1}$ gene showed a nonsignificant ($p$ = .21) but slight increase in expression toward the end of the cells' life span. The expression level of p27 and p53 showed no significant change in vitro (Fig. 3C, 3D).

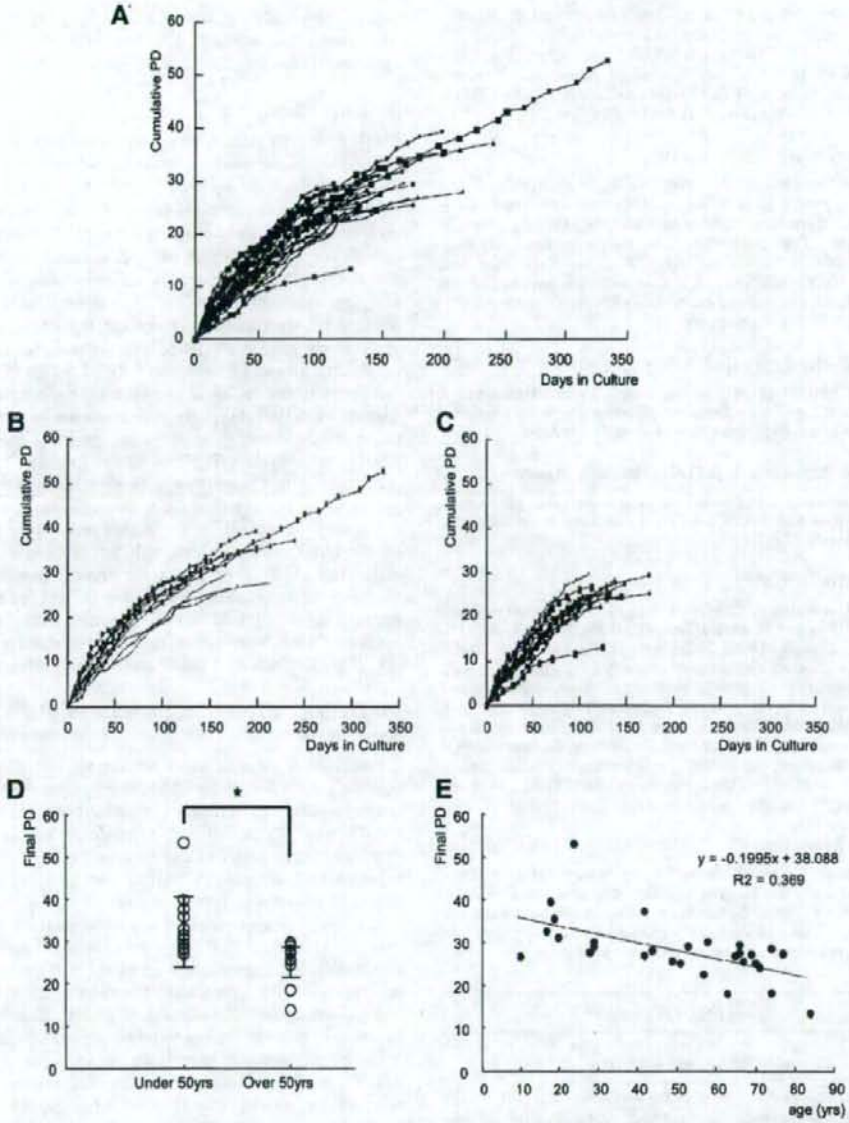


**Figure 1.** Growth profiles of human (h)MSCs in vitro. **(A):** Growth profiles of 29 hMSC strains in vitro. PD number is plotted against culture period. **(B):** Growth profiles of hMSCs from younger donors (<50 years, $n = 13$). **(C):** Growth profiles of hMSCs from older donors (≥50, $n = 16$). **(D):** Comparison of final PD between younger and older donors with Student's $t$ test. There was a significant difference $* p = .0086$. **(E):** A Spearman's rank-correlation coefficient when age was plotted as a metric variable and final PD as an objective variable ($r = -.608$, $p = .00128$). Abbreviations: PD, population doubling; yrs, years.

## The Expression of p16$^{INK4}$ Was Positively Correlated with SA-β-Gal Staining but Not Ki67

Expression of the p16$^{INK4A}$ gene was analyzed at the cellular level using immunocytochemical methods in three randomly selected cases (hMSC08, hMSC40, and hMSC45). The expression of SA-β-gal and Ki67 was also analyzed in these samples as a marker for senescence and proliferation, respectively. Cells positive for p16$^{INK4A}$ were negative for Ki-67 in hMSC08 at PD12, which was 50% of their life span in vitro (final PD number was 25) (Fig. 4Ac). Similar results were obtained in the case of hMSC45 at PD18 (final PD number was 29) (Fig. 4Af) and hMSC40 (data not shown). These data suggested that cells positive for p16$^{INK4A}$ lost their proliferating ability.

Next, SA-β-Gal staining was performed before double staining of p16$^{INK4A}$ and Ki-67, and cells positive for each staining were counted. Among hMSC40 cells at PD6, only 1 of 94 cells (1%) was positive for SA-β-Gal, and it was also stained by

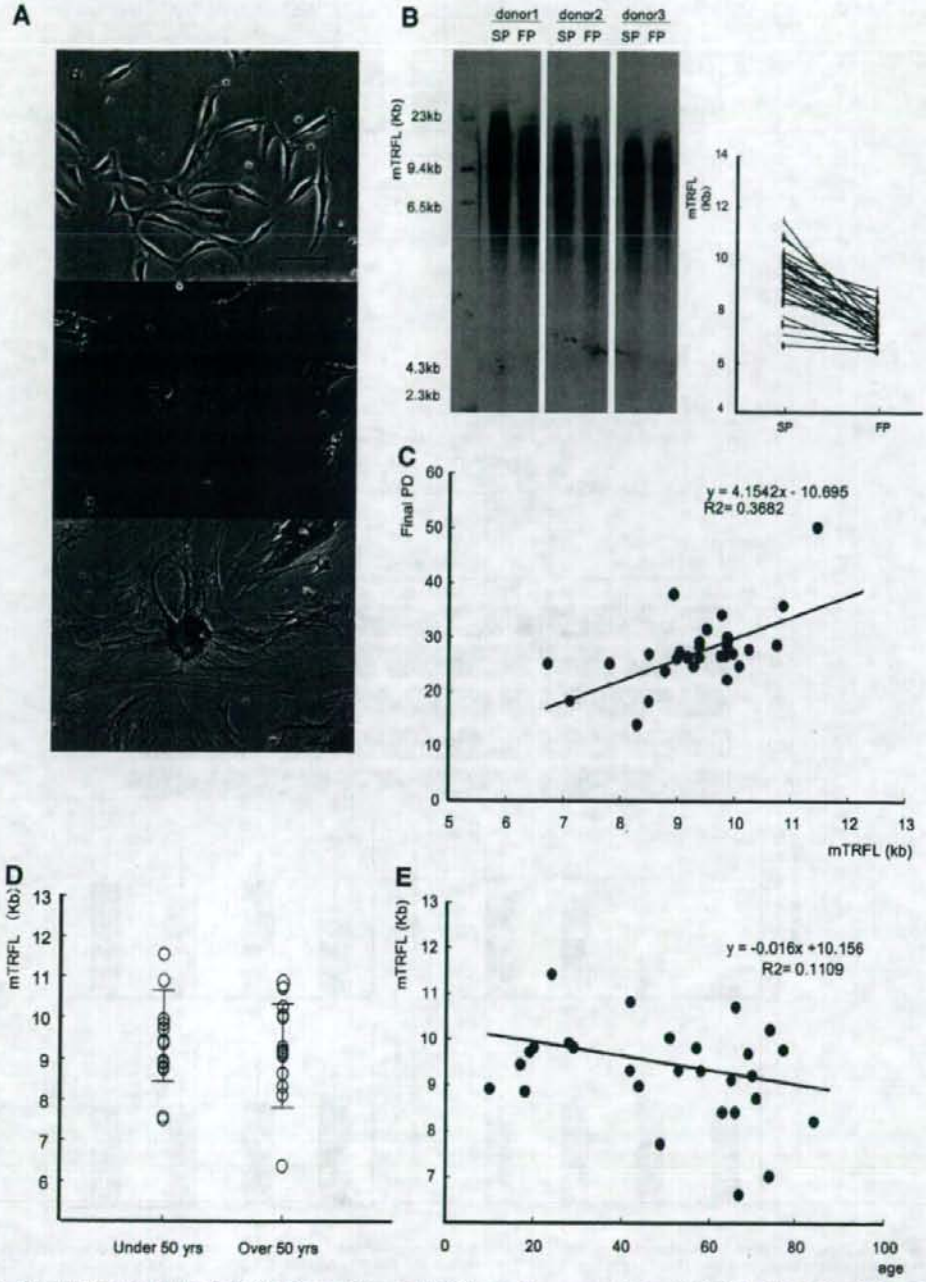


**Figure 2.** Telomere shortening during the in vitro life span of human (h)MSCs. **(A):** Phase-contrast photos of hMSC45 at **(Aa)** PD2 and **(Ab)** PD28. Most cells at PD28 were positive for SA-β-gal staining **(Ac)**; ×400 magnification. Scale bar = 100 μm. **(B):** Detection of telomere restriction fragment by Southern blotting. The mTRFL in the second passage differed among donors (9.4 ± 1.0 kb) but that in late passages converged to almost the same value (7.5 ± 0.6 kb). **(C):** mTRFL at SP as a predictor of the final PD. A statistically significant association ($r = -.557$, $p = .00321$) was obtained with Spearman's rank-correlation coefficient when mTRFL at SP was plotted as a metric variable and final PD as an objective variable. **(D):** Donor age is not a denominator of the mTRFL at SP. No significant difference of mTRFL at SP was observed between younger and older donors ($p = .13$). **(E):** Spearman's rank-correlation coefficient when age was plotted as a metric variable and early mTRFL as an objective variable ($r = -.28$, $p = .13$). Abbreviations: FP, first passage; kb, kilobase; mTRFL, mean telomere restriction fragment length; PD, population doubling; SP, second passage; yrs, years.

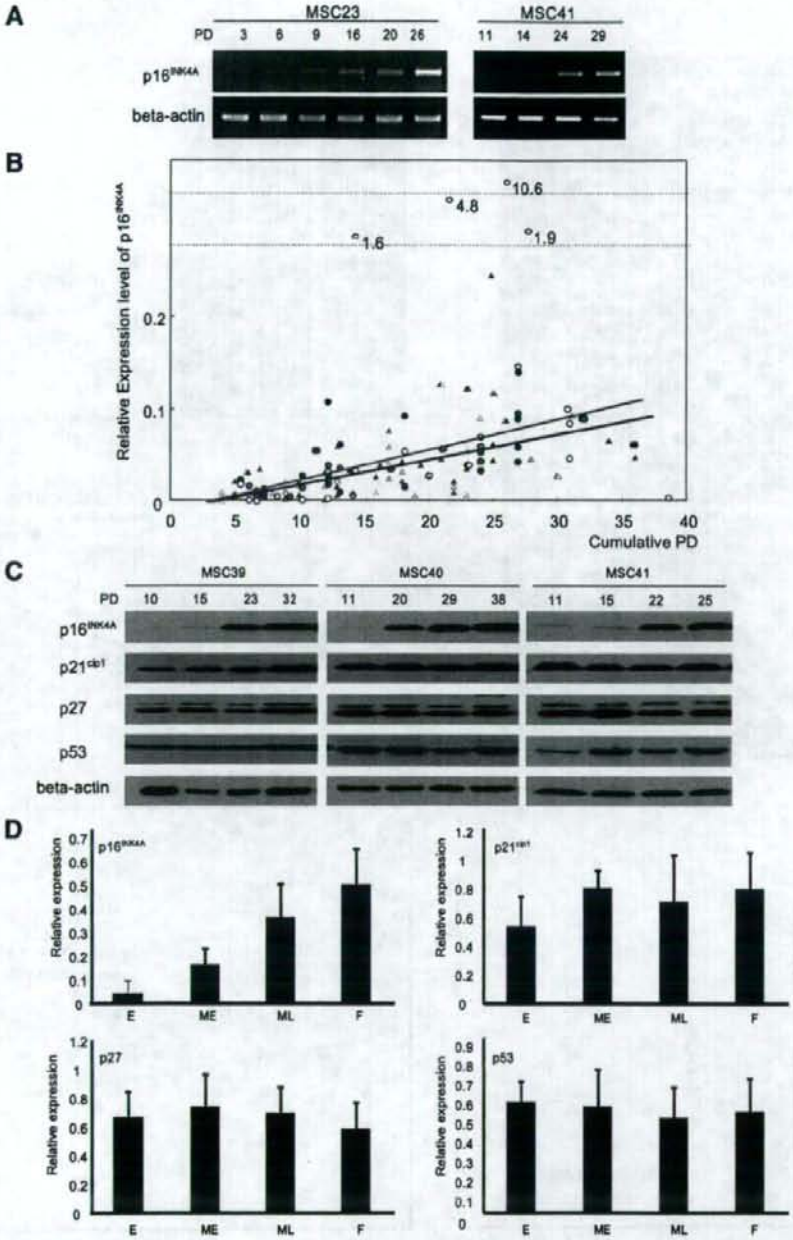


**Figure 3.** PD-dependent increase in the expression of $p16^{INK4A}$. **(A):** mRNA expression of $p16^{INK4A}$ in vitro analyzed by semiquantitative reverse transcription-polymerase chain reaction. **(B):** Correlation of $p16^{INK4A}$ expression with PD number. Samples derived from younger and older donors were demonstrated with circles and triangles, respectively, and samples from each donor taken at different time points are indicated in the same color. PD-dependent expression of $p16^{INK4A}$ was confirmed by multiple regression analysis in human (h)MSC derived from both younger (red line, $r = .59$, $p = .00000015$) and older (blue line, $r = .64$, $p = .0000001$) donors. **(C):** Expression of cell cycle regulators during the in vitro life span of hMSCs. **(D):** Quantitative analyses of the expression of cell cycle regulators in vitro. The relative expression of the cell cycle regulators was quantified as described in Materials and Methods as well as the abbreviation of each time point (E, ME, ML, and F). A significant increase in the expression level of $p16^{INK4A}$ was observed toward the later stage of life (analyzed by one-factor analysis of variance, $p = .00000001$). There was no significant change in vitro in the expression of $p21^{cip1}$ ($p = .21$), p27 ($p = .36$), and p53 ($p = .87$). Abbreviations: E, early; F, final; ME, middle early; ML, middle late; PD, population doubling.

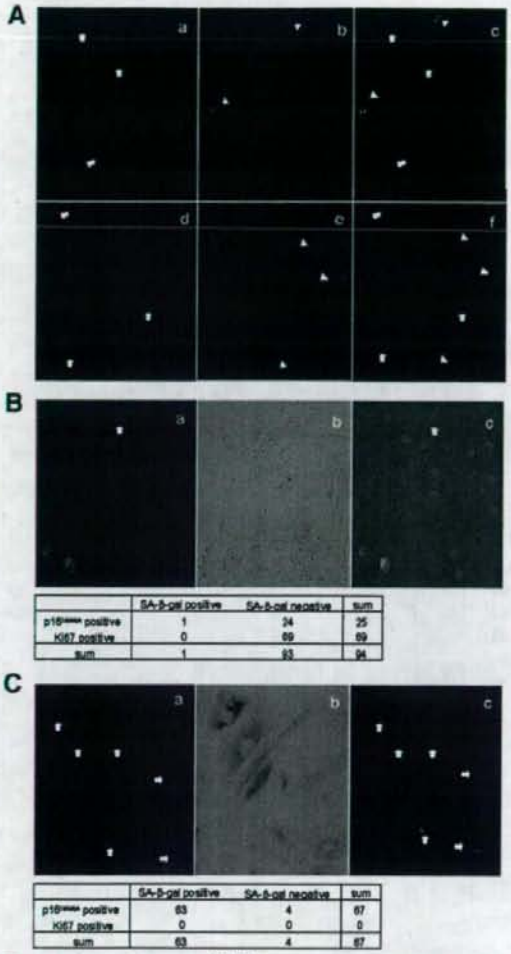


| | SA-β-gal positive | SA-β-gal negative | sum |
|---|---|---|---|
| p16 positive | 1 | 24 | 25 |
| Ki67 positive | 0 | 69 | 69 |
| sum | 1 | 93 | 94 |

| | SA-β-gal positive | SA-β-gal negative | sum |
|---|---|---|---|
| p16 positive | 63 | 4 | 67 |
| Ki67 positive | 0 | 0 | 0 |
| sum | 63 | 4 | 67 |

**Figure 4.** Association of $p16^{INK4A}$ with a marker of senescence but not that of proliferation. **(A):** Immunocytochemical staining of $p16^{INK4A}$ and Ki-67. **(Aa–Ac):** Human (h)MSC08 at population doubling (PD)23 (final PD was 25); **(Ad–Af):** hMSC45 at PD18 (final PD was 26). **(Aa, Ad):** $p16^{INK4A}$ staining. Signals are demonstrated as red dots in nuclei, and arrows indicate positive cells. **(Ab, Ae):** Ki-67 staining. Signals are demonstrated as blue dots in nuclei, and positive cells are indicated by arrowheads. **(Ac, Af):** Merged images. Note that most $p16^{INK4A}$-positive cells were Ki-67-negative and vice versa. **(B):** Triple staining of $p16^{INK4A}$, Ki-67, and SA-β-Gal in hMSC40 at PD6. **(Ba),** double staining of $p16^{INK4A}$ (red) and Ki-67 (green); **(Bb),** light field image of SA-β-Gal staining; **(Bc),** merged image of **(Ba)** and **(Bb).** Cells were classified by staining pattern, and the number of cells in each group is demonstrated in the table below the figures. **(C):** Identical experiments were performed using hMSC40 at a later passage (PD28). Abbreviation: SA-beta-gal, senescence associated-β-galactosidase.

$p16^{INK4A}$ (Fig. 4B). Among SA-β-Gal-negative cells ($n = 93$), 24 (25.8%) were stained with $p16^{INK4A}$ and 69 (73.4%) were stained with Ki67 (Fig. 4B). There were no cells that were double positive for $p16^{INK4A}$ and Ki-67. Among the late passage cells (PD26), 63 (94%) were positive for SA-β-Gal. Among SA-β-Gal-negative cells ($n = 4$), all were stained for $p16^{INK4A}$ and none were stained with Ki67 (Fig. 4C). Identical results were obtained for hMSC08 and hMSC45 (data not shown), and the Mantel-Haenszel chi-squared test with continuity correction in three strains showed a positive correlation between the expression of $p16^{INK4A}$ and SA-β-Gal ($\chi^2 = 2.75$, $p = .046$). These results suggested that $p16^{INK4A}$ expression induced senescence and loss of proliferating ability.

## Knockdown of $p16^{INK4A}$ Rescued Cells from Senescence and Induced Cell Proliferation

To further investigate the role of $p16^{INK4A}$, its expression was inhibited with siRNA. Twenty-four hours after a single transfection with p16-siRNA in $p16^{INK4A}$ positive hMSC (hMSC40 at PD24), effective knockdown of the gene expression was confirmed by RT-PCR, and the expression of the $p14^{ARF}$ gene, which shares exons 2 and 3 with the $p16^{INK4A}$ gene, was not affected by p16-siRNA (Fig. 5A). The knockdown effect at the protein level was confirmed by Western blot analysis (Fig. 5B); no change in the expression level of $p21^{cip1}$ or p53 (Fig. 5B) was observed, indicating a specific effect on the $p16^{INK4A}$ gene.

To investigate the effect of the downregulation of $p16^{INK4A}$ expression on the proliferating ability of hMSC strains that have an upregulated $p16^{INK4A}$, p16-siRNA was introduced into hMSC39 at PD32 (final PD number was 35), and the incorporation of BrdU was assayed 24 hours later. Suppression of $p16^{INK4A}$ gene expression by p16-siRNA was confirmed by RT-PCR (Fig. 5C, lower panel). p16-siRNA treatment led to a 4.2- and 10.5-fold increase in BrdU incorporation compared with no treatment or treatment with control-siRNA, respectively ($p < .01$) (Fig. 5C, upper panel). The knockdown of $p16^{INK4A}$ also rescued cellular senescence. The ratio of SA-β-gal-positive cells treated with p16-siRNA (3.1% ± 0.6%) was significantly lower than that of cells not treated (31.8% ± 5.3%) or treated with control-siRNA (14.2% ± 3.0%) (Fig. 5D). The reason for the decrease in the SA-β-Gal-positive ratio in control-siRNA treated cells is probably due to the decrease in total cell number (nontreatment group: 164 ± 25.7, control-siRNA group: 112.7 ± 19.4, p16-siRNA group: 172.3 ± 38.6). Senescent cells expressing SA-β-Gal seemed to be vulnerable to the trypsinization process, which was required for the transfection experiments. Even in such a situation, the total cell number was increased in the p16-siRNA group. The growth stimulatory effect of p16-siRNA was confirmed by serial cell counting (Fig. 5E). The fold increase in cell number at 144 and 216 hours after transfection was higher in the p16-siRNA-treated cells than in cells without treatment or control-siRNA-treated cells (Fig. 5E).

## The Expression Profile of $p16^{INK4A}$ Is Classified into Three Types

In almost all strains, the expression of $p16^{INK4A}$ gradually increased with the propagation in vitro (Fig. 3) of hMSC10, shown in Figure 6C. There were, however, some strains showing a different profile of expression. Based on the $p16^{INK4A}$ expression profile in vitro, 29 cases were divided into three groups and analyzed in detail (supplemental online Table 1).

***Gradual Increase Group.*** Twenty-five of 29 (86%) strains demonstrated this pattern of expression (Fig. 6A; hMSC23 shown in Fig. 6A). The expression level at the final passage was at least two times higher than at the first passage. The mean final PD of the gradual increase (GI) group was 28.1 ± 7.2 (18–39), and the mean culture period was 151.2 ± 47.7 days (90–240 days). The mTRFL of SP was 9.4 ± 1.0 kb (6.7–10.1 kb) and that of FP was 7.5 ± 0.6 kb (6.4–8.5 kb). The mean highest expression of $p16^{INK4A}$ was 0.06 ± 0.04 (0.019–0.24). The expression of $p16^{INK4A}$ was not increased more than 0.3 relative

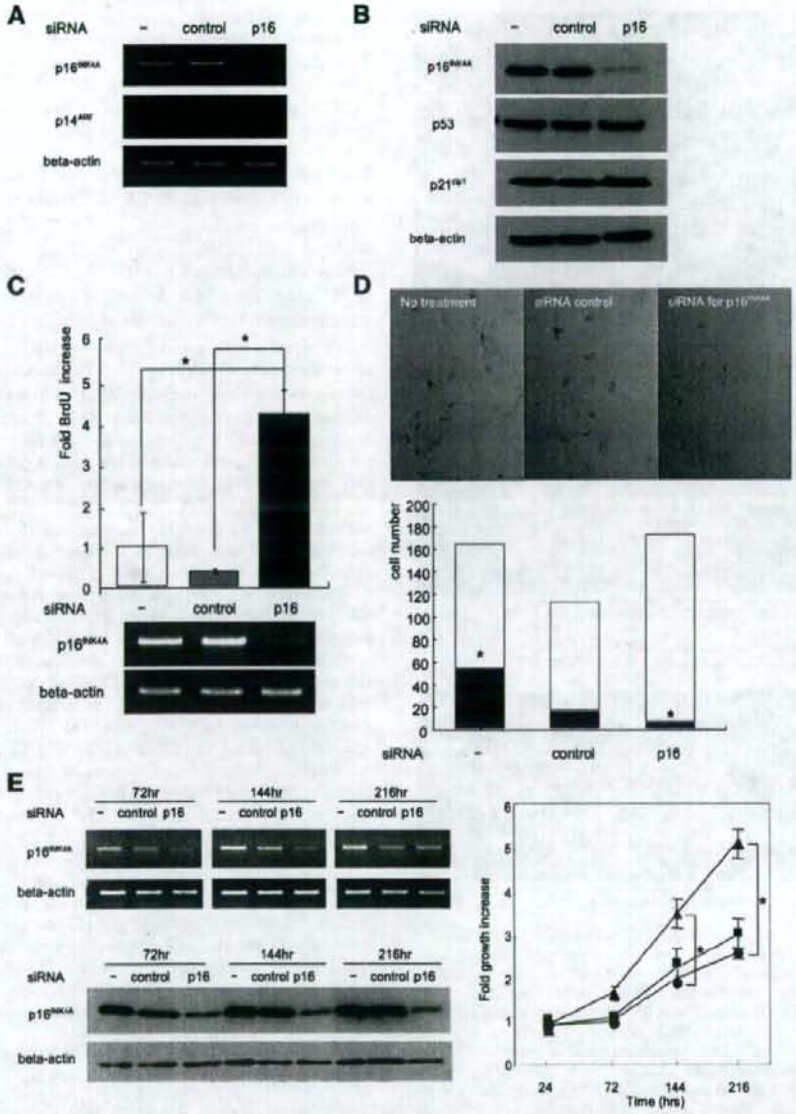


**Figure 5.** Knockdown of $p16^{INK4A}$ prevented senescence and restored proliferation. **(A):** Inhibition of $p16^{INK4A}$ gene expression by p16-siRNA. siRNA for a scramble sequence (control-siRNA) was used as a control. **(B):** Specific inhibition of p16 protein expression by p16-siRNA. **(C):** Incorporation of BrdU after siRNA treatment. Effective inhibition of $p16^{INK4A}$ expression by p16-siRNA was confirmed by reverse transcription-polymerase chain reaction shown in the lower part of the figure; *, $p < .01$. **(D):** Senescence associated-β-galactosidase (SA-β-Gal) staining after siRNA treatment. Representative data were shown in the upper part of the figure, and SA-β-Gal-positive (black square) and negative (white square) cells were counted as described in the Materials and Methods section and are shown in the lower part; *, $p < .01$. Note that total cell number was decreased in the control-siRNA-treated cells, whereas the number in the p16-siRNA-treated cells was equal to that in untreated cells. **(E):** Growth profile of human MSCs after siRNA treatment. Living cells of each group (▲, treated with p16-siRNA; ●, treated with control-siRNA; ■, no treatment) were numerated at each time point, and the fold increase compared with the number at 24 hours after siRNA treatment was demonstrated; *, $p < .01$. Abbreviations: BrdU, 5-bromo-2′-deoxyuridine; hr(s), hours; siRNA, small interfering RNA.

to the expression of Suos2. The expression level of the BMI1 gene showed no significant change in vitro (Fig. 6Ab).

***Increase Followed by Reduction Group.*** Two out of 29 (7%) strains showed a rapid reduction in $p16^{INK4A}$ gene expression after an extremely high level was reached (Fig. 6B; hMSC17 shown in Fig. 6B; hMSC14, data not shown). The donor age was relatively young (hMSC14, 17 years; hMSC17, 24 years). The final PD (hMSC14, 33; hMSC17, 54) and culture period (hMSC14, 147 days; hMSC17, 334 days) were lengthened. The mTRFL of SP was almost equal to the average of the GI group

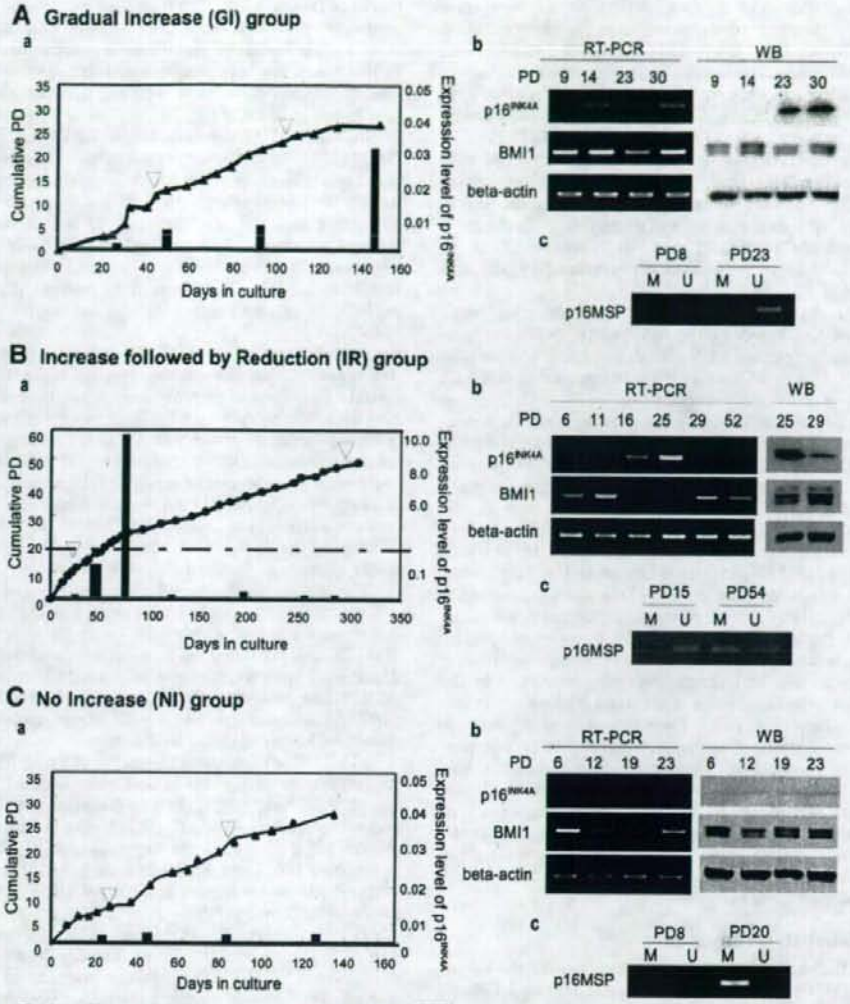


**Figure 6.** Classification of human (h)MSC strains by the expression of $p16^{INK4A}$ during cell expansion. **(A):** GI group. **(Aa):** Cumulative PD (line graph) and the relative expression of the $p16^{INK4A}$ gene (bar graph) in hMSC23. The arrowhead indicates the time point at which the methylation of the $p16^{INK4A}$ gene was analyzed. **(Ab):** Expression of the $p16^{INK4A}$ and BMI1 genes at the mRNA (left panel) and protein (right panel) levels. **(Ac):** MSP of the $p16^{INK4A}$ gene. **(B):** IR group. Samples were derived from hMSC17. **(C):** NI group. Samples were derived from hMSC10. Abbreviations: GI, gradual increase; IR, increase followed by reduction; M, fragments amplified by methylated sequence-specific primers; MSP, methylation-specific polymerase chain reaction; NI, no increase; PD, population doubling; RT-PCR, reverse transcription-polymerase chain reaction; U, fragments amplified by unmethylated sequence-specific primers; WB, western blotting.

in hMSC14 (9.5 kb) but longer in hMSC17 (11.5 kb). The mTRFL of FP was equal to the average of the GI group in both strains (hMSC14, 7.6 kb; hMSC17, 6.9 kb). The highest value of $p16^{INK4A}$ expression was much higher than the mean value of the GI group in both strains (hMSC14, 4.8; hMSC17, 10.6). Interestingly, the expression of the BMI1 gene was repressed during the period in which the expression level of the $p16^{INK4A}$ gene was extremely high and returned to the initial level after the $p16^{INK4A}$ gene was downregulated (Fig. 6Bb).

***No Increase Group.*** In two out of 29 (7%) strains, the level of $p16^{INK4A}$ remained low throughout the culture (hMSC10 shown in Fig. 6C; hMSC24, data not shown). The final PD (hMSC10, 28; hMSC24, 27) and culture period (hMSC10, 138 days; hMSC24, 170 days) were almost equal to the average for the GI group. The mTRFL of SP was almost equal to the average of the GI group in both strains (hMSC10: 10.3 kb, hMSC24: 9.0 kb). The mTRFL of FP was longer in hMSC10 (8.5 kb) but equal in hMSC24 (7.1 kb). The highest expression of $p16^{INK4A}$ did not exceed 0.01 (hMSC10, 0.0063; hMSC25, 0.0028). The expression level of the BMI1 gene showed no significant change during the culture period.

## Methylation of the Promoter of the $p16^{INK4A}$ Gene

Several mechanisms were found as the cause of downregulation of the $p16^{INK4A}$ expression in cancer cells, the DNA methylation in the core promoter region being the most frequent event

[28]. Several experiments were performed to investigate whether DNA methylation was involved in the downregulation of $p16^{INK4A}$ expression observed in certain hMSC strains. First, hMSC17 cells, one of two strains in the increase-followed-by-reduction (IR) group, were treated with the demethylation drug 5-aza-dC for 96 hours, and $p16^{INK4A}$ expression was checked by RT-PCR (supplemental Fig. 2). As seen in control U2OS cells, an osteosarcoma cell line in which $p16^{INK4A}$ expression is downregulated by DNA methylation [32], $p16^{INK4A}$ expression was induced in PD54 but not in PD15 (supplemental online Fig. 2A). 5-aza-dC treatment also induced a senescence phenotype in late passage hMSC17 (PD54) as SA-$\beta$-Gal-positive cells increased by twofold after 96 hours of treatment (supplemental Fig. 2B).

Next, the methylation status of the promoter region of $p16^{INK4A}$ was analyzed by the MSP assay. MSP was performed using the genomic DNA from early and late passage cells from 10 strains of the GI group, in two strains of the IR group, and in two strains of the no increase (NI) group (supplemental online Table 1). The methylated sequence-specific fragment of the $p16^{INK4A}$ gene was not amplified in 12 out of 12 group GI strains either in early or late passage cells, and unmethylated sequence-specific fragments were amplified (Fig. 6Ac). In the case of hMSC17 from the IR group, only unmethylated sequence-specific fragments were amplified using DNA extracted from cells at PD15, at which the level of $p16^{INK4A}$ expression remained low (Fig. 6Bc). When DNA extracted from cells at PD54 was used for MSP, however, methylated sequence-specific fragments were amplified, and the amount of unmethylated sequence-specific fragments decreased (Fig. 6Bc). In the NI group, the methylated sequence-specific fragment was observed even in the early passage cells in addition to the unmethylated sequence-specific fragment (Fig. 6Cc). The expression of the methylated sequence-specific fragment was increased in late passage, and unmethylated sequence-specific fragment was decreased. Methylation of the target region of MSP in these samples was confirmed by bisulfite sequencing (data not shown). These results indicated that DNA methylation in the core promoter region plays a role in downregulating the expression of the $p16^{INK4A}$ gene in vitro in hMSCs as observed in human cancers.

### Chromosomal Rearrangement

Because of the extraordinarily long culture period, the karyotype of hMSC17 was analyzed using the standard G-band method, and several samples from the GI and NI groups were also analyzed. No chromosomal aberrations were detected in samples from the GI and NI groups (data not shown). The chromosomal structure was also normal in hMSC17 at early passage (PD10) (supplemental online Fig. 3A). Cells of the same strain at the later passage (PD54), however, showed a number of numerical and structural aberrations including two clonal aberrations with the same reciprocal translocation (supplemental online Fig. 3B). Therefore, both epigenetic and genetic abnormalities existed in the late passage cells of hMSC17, which might be responsible for the prolonged culture of this strain.

## DISCUSSION

Unlimited self-renewal ability is a hallmark of embryonic stem cells, providing the potential to differentiate into cells of any type [33]. In the case of tissue stem cells including MSCs, however, the potential to proliferate is restricted in the Hayflick model of cellular aging. The molecular mechanism for inducing senescence in vitro has been extensively investigated, and recent reports suggested a cell specificity-dependent mechanism [33]. In this study, we have demonstrated that telomere length and $p16^{INK4A}$ expression are involved in different phases of cellular senescence in hMSC.

In human MSCs, telomerase activity was not detected [26, 34]. The mean telomere restriction fragment length in primary hMSCs was 9.4 $\pm$ 1.0 kb for early passage and 7.5 $\pm$ 0.6 kb for late passage cells, and the mean telomere shortening rate was 109 $\pm$ 43 bp (Fig. 2), which is close to the theoretical length of shortening in each DNA replication, suggesting that there is no mechanism to maintain telomere length in hMSCs. Therefore, it is rational that the initial mTRFL correlated well with the replicative capacity of hMSCs ($r$ = .677, Fig. 2C). hMSCs transduced with the human telomerase gene hTERT exhibit a prolonged replicative capacity, evidence that the integrity of the telomere plays a vital role in regulating replicative capacity in vitro [26, 35]. However, the shortening of telomeres is not the sole factor inducing cellular senescence in hMSCs, and our current results indicated that the upregulation of the $p16^{INK4A}$ gene expression plays an essential role in this process. This may be relevant to our previous data that the introduction of hTERT was not sufficient to immortalize hMSC, and that the inactivation of the function of p16 either by the HPVE6/E7 or BMI1 genes was required [26, 36].

The relationship between growth capacity and donor age is not clear. Clearly, the hMSC strains isolated from younger donors on the average exhibited a longer life span in vitro (Fig. 1D, 1E), and the initial mTRFL correlated with the life span. There was, however, no clear relationship between the initial mTRFL and donor age (Fig. 2). Also, the expression profile of $p16^{INK4A}$ was not correlated with donor age. These issues should be further analyzed in detail.

$p16^{INK4A}$ is known as a biomarker of aging. This cell cycle regulator is not expressed in undifferentiated hESCs [37]. In mouse HSCs and NSCs, the expression of $p16^{INK4A}$ was repressed by the PcG protein BMI1 [15]. But in later life, this PcG protein failed to repress the expression of $p16^{INK4A}$ and the function of HSCs and NSCs declined [14, 15]. In the current study, BMI1 was expressed at the mRNA and protein levels in all the hMSC strains (Fig. 6). In some strains, the expression of BMI1 was negatively correlated with the expression of $p16^{INK4A}$ (Fig. 6B, 6C). The relationship between these two molecules in hMSCs remained to be investigated. The expression of $p16^{INK4A}$ was increased toward senescence (Fig. 3), and senescent cells expressed $p16^{INK4A}$. The downregulation of $p16^{INK4A}$ expression resulted in escape from senescence and a restoration of the proliferating activity (Fig. 5). These results suggest that most hMSCs do not have a mechanism to repress the expression of $p16^{INK4A}$ in vitro.

We found three types of passage-dependent change of the p16 gene expression during in vitro life of hMSCs of which two were associated with the methylation-induced suppression. No clear differences were found among three groups in clinical characters of donors, and the procedures for the isolation and expansion of hMSCs were the same in all cases. Subtle changes in the culture condition such as the initial density, the concentration of $CO_2$, and the timing of passage may influence the development of the methylation, which will be an important issue to be further investigated.

As far as we know, this is the first report to demonstrate the methylation of $p16^{INK4A}$ in hMSCs. This phenomenon was observed in 4 of 29 strains (13.8%), which is above the negligible frequency (Fig. 6, supplemental online Table 1). Methylation of the $p16^{INK4A}$ gene in normal cells in vitro is reported in

the case of human mammary epithelial cells showing a prolonged life span in vitro [20]. In many cases, however, this phenomenon is seen in cancer cells [38].

A line of evidence has indicated a tight association between the inactivation of $p16^{INK4A}$ and transformation of hMSCs. The hMSCs immortalized with hTERT showed spontaneous transformation in vitro in association with the deletion of the $p16^{INK4A}$ gene and activation of the K-*ras* gene [39]. The hMSC strain transformed spontaneously in vitro lacked expression of the $p16^{INK4A}$ gene [24]. The BMI1-transduced immortalized hMSCs, which showed no detectable $p16^{INK4A}$ gene expression, became fully transformed after the introduction of an activated H-*ras* gene [36]. In this study, one case with an inactivated $p16^{INK4A}$ gene by DNA methylation (hMSC17) showed a prolonged life span (334 days in culture with a final PD of 54) in vitro far longer than the average (151 days and 28 PD) (Fig. 6Bb). Although no apparent phenotype of transformed cells was observed in this strain, and the growth ceased with telomere shortening, the association of chromosomal aberrations (supplemental online Fig. 3) may be considered a sign of pretransformation as reported in human and murine MSC cases [24, 40, 41]. This point should be seriously considered in the clinical use of hMSCs, particularly in cases requiring prolonged and extensive in vitro expansion. Monitoring of the DNA methylation of the $p16^{INK4A}$ gene will serve as surveillance for the transformation of hMSCs.

## ACKNOWLEDGMENTS

The authors thank Drs. Tohru Kiyono, Koichi Nishijo, Satoshi Teramukai, and Tatsuya Ishibe for advice and Drs. Takeshi Sakamoto and Hiromu Ito for clinical samples. This work was supported by the New Energy and Industrial Technology Development Organization (NEDO), with a project entitled Development of Evaluation Technology for Early Introduction of Regenerative Medicine, and also by Grants-in-aid for Scientific Research from the Japan Society for the Promotion of Science, from the Ministry of Education, Culture, Sports, Science, and Technology, and from the Ministry of Health, Labor, and Welfare.

## DISCLOSURE OF POTENTIAL CONFLICTS OF INTEREST

The authors indicate no potential conflicts of interest.

## REFERENCES

1 Caplan AI, Bruder SP. Mesenchymal stem cells: Building blocks for molecular medicine in the 21st century. Trends Mol Med 2001;7:259–264.
2 Mazzini L, Mareschi K, Ferrero I et al. Autologous mesenchymal stem cells: Clinical applications in amyotrophic lateral sclerosis. Neurol Res 2006;28:523–526.
3 Ohgushi H, Kotobuki N, Funaoka H et al. Tissue engineered ceramic artificial joint—ex vivo osteogenic differentiation of patient mesenchymal cells on total ankle joints for treatment of osteoarthritis. Biomaterials 2005;26:4654–4661.
4 Deans RJ, Moseley AB. Mesenchymal stem cells: Biology and potential clinical uses. Exp Hematol 2000;28:875–884.
5 Hayflick L, Moorhead PS. The serial cultivation of human diploid cell strains. Exp Cell Res 1961;25:585–621.
6 Itahana K, Campisi J, Dimri GP. Mechanisms of cellular senescence in human and mouse cells. Biogerontology 2004;5:1–10.
7 Blackburn EH. Telomere states and cell fates. Nature 2000;408:53–56.
8 Harley CB, Futcher AB, Greider CW. Telomeres shorten during ageing of human fibroblasts. Nature 1990;345:458–460.
9 Carpenter MK, Rosler ES, Fisk GJ et al. Properties of four human embryonic stem cell lines maintained in a feeder-free culture system. Dev Dyn 2004;229:243–258.
10 Miura T, Luo Y, Khrebtukova I et al. Monitoring early differentiation events in human embryonic stem cells by massively parallel signature sequencing and expressed sequence tag scan. Stem Cells Dev 2004;13:694–715.
11 Allsopp RC, Cheshier S, Weissman IL. Telomere shortening accompanies increased cell cycle activity during serial transplantation of hematopoietic stem cells. J Exp Med 2001;193:917–924.
12 Serrano M, Hannon GJ, Beach D. A new regulatory motif in cell-cycle control causing specific inhibition of cyclin D/CDK4. Nature 1993;366:704–707.
13 Krishnamurthy J, Torrice C, Ramsey MR et al. INK4A/Arf expression is a biomarker of aging. J Clin Invest 2004;114:1299–1307.
14 Janzen V, Forkert R, Fleming HE et al. Stem-cell ageing modified by the cyclin-dependent kinase inhibitor $p16^{INK4A}$. Nature 2006;443:421–426.
15 Molofsky AV, Slutsky SG, Joseph NM et al. Increasing $p16^{INK4A}$ expression decreases forebrain progenitors and neurogenesis during ageing. Nature 2006;443:448–452.
16 Park IK, Morrison SJ, Clarke MF. Bmi1, stem cells, and senescence regulation. J Clin Invest 2004;113:175–179.
17 Park IK, Qian D, Kiel M et al. Bmi-1 is required for maintenance of adult self-renewing haematopoietic stem cells. Nature 2003;423:302–305.
18 Molofsky AV, Pardal R, Iwashita T et al. Bmi-1 dependence distinguishes neural stem cell self-renewal from progenitor proliferation. Nature 2003;425:962–967.
19 Jacobs JJ, Kieboom K, Marino S et al. The oncogene and Polycomb-group gene bmi-1 regulates cell proliferation and senescence through the INK4A locus. Nature 1999;397:164–168.
20 Wong DJ, Foster SA, Galloway DA et al. Progressive region-specific de novo methylation of the p16 CpG island in primary human mammary epithelial cell strains during escape from M0 growth arrest. Mol Cell Biol 1999;19:5642–5651.
21 Holliday R, Grigg GW. DNA methylation and mutation. Mutat Res 1993;285:61–67.
22 Ushijima T, Okochi-Takada E. Aberrant methylations in cancer cells: Where do they come from? Cancer Sci 2005;96:206–211.
23 Ushijima T, Nakajima T, Maekita T. DNA methylation as a marker for the past and future. J Gastroenterol 2006;41:401–407.
24 Rubio D, Garcia-Castro J, Martin MC et al. Spontaneous human adult stem cell transformation. Cancer Res 2005;65:3035–3039.
25 Caterson EJ, Nesti LJ, Danielson KG et al. Human marrow-derived mesenchymal progenitor cells: Isolation, culture expansion, and analysis of differentiation. Mol Biotechnol 2002;20:245–256.
26 Okamoto T, Aoyama T, Nakayama T et al. Clonal heterogeneity in differentiation potential of immortalized human mesenchymal stem cells. Biochem Biophys Res Commun 2002;295:354–361.
27 Huang HJ, Yee JK, Shew JY et al. Suppression of the neoplastic phenotype by replacement of the RB gene in human cancer cells. Science 1988;242:1563–1566.
28 Herman JG, Graff JR, Myohanen S et al. Methylation-specific PCR: A novel PCR assay for methylation status of CpG islands. Proc Natl Acad Sci U S A 1996;93:9821–9826.
29 Dimri GP, Lee X, Basile G et al. A biomarker that identifies senescent human cells in culture and in aging skin in vivo. Proc Natl Acad Sci U S A 1995;92:9363–9367.
30 Flores I, Cayuela ML, Blasco MA. Effects of telomerase and telomere length on epidermal stem cell behavior. Science 2005;309:1253–1256.
31 Bodnar AG, Ouellette M, Frolkis M et al. Extension of life-span by introduction of telomerase into normal human cells. Science 1998;279:349–352.
32 Park YB, Park MJ, Kimura K et al. Alterations in the INK4a/ARF locus and their effects on the growth of human osteosarcoma cell lines. Cancer Genet Cytogenet 2002;133:105–111.
33 Rosler ES, Fisk GJ, Ares X et al. Long-term culture of human embryonic stem cells in feeder-free conditions. Dev Dyn 2004;229:259–274.
34 Sethe S, Scutt A, Stolzing A. Aging of mesenchymal stem cells. Ageing Res Rev 2006;5:91–116.
35 Simonsen JL, Rosada C, Serakinci N et al. Telomerase expression extends the proliferative life-span and maintains the osteogenic potential of human bone marrow stromal cells. Nat Biotechnol 2002;20:592–596.

36 Shima Y, Okamoto T, Aoyama T et al. In vitro transformation of mesenchymal stem cells by oncogenic H-rasVal12. Biochem Biophys Res Commun 2007;353:60–66.
37 Zeng X, Rao MS. Human embryonic stem cells: Long term stability, absence of senescence and a potential cell source for neural replacement. Neuroscience 2007;145:1348–1358.
38 Rocco JW, Sidransky D. p16(MTS-1/CDKN2/$^{INK4A}$) in cancer progression. Exp Cell Res 2001;264:42–55.
39 Serakinci N, Guldberg P, Burns JS et al. Adult human mesenchymal stem cell as a target for neoplastic transformation. Oncogene 2004;23: 5095–5098.
40 Zhou YF, Bosch-Marce M, Okuyama H et al. Spontaneous transformation of cultured mouse bone marrow-derived stromal cells. Cancer Res 2006;66:10849–10854.
41 Tolar J, Nauta AJ, Osborn MJ et al. Sarcoma derived from cultured mesenchymal stem cells. STEM CELLS 2007;25:371–379.

See www.StemCells.com for supplemental material available online.

Available online at www.sciencedirect.com
ScienceDirect
ELSEVIER
Biochemical and Biophysical Research Communications 365 (2008) 124–130
BBRC
www.elsevier.com/locate/ybbrc

# Cell-specific epigenetic regulation of ChM-I gene expression: Crosstalk between DNA methylation and histone acetylation

Tomoki Aoyama [a,*], Takeshi Okamoto [a,b,1], Yoshiki Kohno [a,b], Kenichi Fukiage [a], Seiji Otsuka [a,c], Moritoshi Furu [a], Kinya Ito [a,c], Yonghui Jin [a], Satoshi Nagayama [d], Tomitaka Nakayama [b], Takashi Nakamura [b], Junya Toguchida [a]

[a] *Institute for Frontier Medical Sciences, Kyoto University, Kyoto, Japan*
[b] *Department of Orthopaedic Surgery, Graduate School of Medicine, Kyoto University, Kyoto, Japan*
[c] *Department of Musculoskeletal Medicine, Graduate School of Medical Sciences, Nagoya City University, Nagoya, Japan*
[d] *Department of Surgery and Surgical Basic Science, Graduate School of Medicine, Kyoto, Japan*

Received 19 October 2007
Available online 31 October 2007

**Abstract**

The expression of the chondromodulin-I (ChM-I) gene, a cartilage-specific gene, is regulated by the binding of Sp3 to the core promoter region, which is inhibited by the methylation of CpG in the target genome in the osteogenic lineage, osteosarcoma (OS) cells. The histone tails associated with the hypermethylated promoter region of the ChM-I gene were deacetylated by histone deacetylase 2 (HDAC2) in three ChM-I-negative OS cell lines. Treatment with an HDAC inhibitor induced the binding of Sp3 in one cell line, which became ChM-I-positive. This process was associated with acetylation instead of the dimethylation of histone H3 at lysine 9 (H3-K9) and, surprisingly, the demethylation of the core promoter region. The demethylation was transient, and gradually replaced by methylation after a rapid recovery of histone deacetylaion. These results represent an example of the plasticity of differentiation being regulated by the cell-specific plasticity of epigenetic regulation.


*Keywords:* Chondromodulin-I; Histone modification; Acetylation; Differentiation; Epigenetic; Chondrogenic; Methylation; H3-K9; HDAC2

The expression of cell type-specific genes is tightly regulated by a hierarchical mechanism composed of genetic and epigenetic factors. In some cases, a single transcription factor may determine cell fate. In other instances, however, the expression of such a master gene is found in cells in other tissue-lineages. For example, the expression of the SOX9 gene, which is the master gene for chondrogenic cell lineage, is also found of in cells of the ostogenic lineage [1]. Transcription factors regulating the expression positively or negatively must bind to specific DNA elements to exert their function, and the factors regulating such binding significantly affect their function and therefore the expression of each gene.

Chondromodulin-I (ChM-I) is a potent vascular endothelial cell growth inhibitor purified from bovine epiphyseal cartilage [2], the expression of which in matured limbs is limited to cells in the resting, proliferating, and early hypertrophic zone of the growth plate [2], and not in other mesenchymal tissues including bone. Therefore, it is a suitable material for analyzing the molecular mechanism regulating cell-specific genes, and we have shown that the Sp3 transcription factor is a major driver of binding to a specific portion in the core promoter region [1]. Because Sp3 is a universal transcription factor ubiquitously expressed in many tissues, the cell-specific expression of the ChM-I gene requires additional factors. Using osteosarcoma (OS) cells, which are malignant mesenchymal

* Corresponding author. Fax: +81 75 751 4646.
*E-mail address:* blue@frontier.kyoto-u.ac.jp (T. Aoyama).
[1] Present address: Department of Orthopaedic Surgery, Kitano Hospital, 2-4-20 Ohgimachi, Kita-ku, Osaka 530-8480, Japan.

0006-291X/$ - see front matter © 2007 Elsevier Inc. All rights reserved.
doi:10.1016/j.bbrc.2007.10.135

tumor cells with features of osteogenic lineage cells, we have shown that DNA methylation of the Sp3-binding sequence is one such mechanism to shut down the expression in cells of the osteogenic lineage [1]. Treatment with a demethylating reagent, however, failed to restore the expression of the ChM-I gene in some OS cells, suggesting the presence of other regulatory mechanisms [1].

Modification of the histone tail is another epigenetic regulatory mechanism [3]. Histone proteins assemble into nucleosomes, which function as DNA packaging. The amino-terminal tails of histone protrude from the nucleosome and are subject to chemical modifications including phosphorylation, ubiquitination, acetylation, and methylation [4]. The acetylation of lysine residues on histone H3 and H4 leads to the formation of an open chromatin structure and allows regulatory factors to easily access the chromatin [4], which is regulated by the stochastic balance of histone acetyltrasferases (HAT) and histone deacetylases (HDAC). Notably, dimethylation of histone H3 at lysine 9 (H3-K9) tightly inhibits the gene expression, correlated with the methylation of CpG [5,6]. These modifications of the histone tail and CpG methylation status determine the differentiation [7].

Here, we investigated the epigenetic regulation of the ChM-I gene in a variety of OS cell lines and found that modifications of the histone tail determine the expression. We found evidence for crosstalk between the modification of histones and methylation of CpG, in which histone acetylation can inhibit the maintenance of CpG methylation by substituting H3-K9 dimethylation with H3-K9 acetylation.

## Materials and methods

*Cell lines and culture conditions.* The human cell lines Saos2, HuO, HOS, MG63, and U2OS were obtained from ATCC or Japanese Cancer Research Resources Bank. The human osteosarcoma cell lines TAKAO and ANOS were established in our laboratory. All the cell lines used in this study were maintained in DMEM (Sigma) with 10% fetal bovine serum (Hyclone, South Logan, UT), 100 U/ml penicillin, and 100 mg/ml streptomycin, in 5% $CO_2$ at 37 °C.

*SDS–PAGE.* Western blotting was performed as previously mentioned [1]. The primary antibodies used were as follows: acetylated H3, acetylated H4, dimethylated H3-K9, acetylated H3-K9, and H3 from Upstate Biotechnology (Lake Placid, NY), HDAC2, HDAC3, and HDAC6 from Zymed Laboratory (San Francisco, CA), and Sp1 and Sp3 from Santa Cruz Biotechnology (Santa Cruz, CA).

*Reverse transcription (RT)-PCR and quantitative RT-PCR.* RNA was isolated using Trizol Reagent (Life Technologies, Rockville, MD) following the manufacturer's directions from frozen tumor tissues and the cultured cell lines. All RT reactions were performed using 1 μg of total RNA with a Super Script First Strand Synthesis System for RT-PCR kit (Life Technologies) according to the instructions supplied. RT-PCR amplification was performed as previously mentioned [1].

*Demethylation drug treatment.* The cells ($1 \times 10^5$) were seeded on 60-mm dishes in DMEM with 10% FBS. After cells attaching to the dishes, the cells were treated with 1 μM of 5-Aza-2′-deoxycytidine (5-Aza-dC) (Sigma–Aldrich) for 96 h.

*Histone deacetylase inhibitor (HDACi) treatment.* The cells ($1 \times 10^5$) were seeded on 60-mm dishes in DMEM with 10% FBS. After attaching to the dishes, they cells were treated with histone deacetylase inhibitors; MS-275 provided by Nihon Scherring (Chiba, Japan), The cells were harvested after 24 h.

*Bisulfite genomic sequencing.* The bisulfite modification of DNA samples was performed using the EpiTect bisulfite kit (Qiagen, Tokyo, Japan). Bisulfite-modified DNA spanning residues −297 to −104 relative to the transcription start point [1] was amplified, cloned into the TA-vector (Invitrogen), and sequenced using an ABI 377 semiautomatic sequencer (PE Applied Biosystems).

*Chromatin immunoprecipitation (ChIP).* The suitability of each antibody for the ChIP assay was confirmed by immunoprecipitation–Western blotting (data not shown). Tissue samples were treated using an EpiQuik tissue ChIP kit according to the manufacturer's directions (Epigentek Group Inc. Brooklyn, NY). Cells were harvested and mixed with formaldehyde at a final concentration of 1.0% for 10 min at 37 °C to cross-link protein to DNA. Cells then were suspended in 0.2 ml of SDS lysis buffer and settled on ice for 10 min. DNA cross-linked with protein was sonicated into fragments of 200–1000 bp. One-tenth of the sample was set aside as an input control, and the rest was precleared with salmon sperm DNA protein A–Sepharose beads (Upstate Biotechnology) for 30 min with agitation. The soluble chromatin fraction was collected with each antibody at 4 °C overnight with rotation. Immune complexes were collected with salmon sperm DNA protein A–Sepharose beads and washed with the manufacturer's low salt, high salt, and LiCl buffers and then washed twice with TE buffer (10 mM Tris–HCl and 1 mM EDTA). The chromatin-antibody complexes were eluted with elution buffer (1% SDS and 0.1 M $NaHCO_3$). Protein–DNA cross-links were reversed with 5 M NaCl at 65 °C for 4 h, proteinase K treatment and phenol–chloroform extraction were carried out, and then the DNA was precipitated in ethanol. PCR amplification was performed using primers specific for the *ChM-I* promoter (sense, 5-GAATGCAGGCCAGTGAGAAGGT-3; antisense, 5-GCACCCTGGGATCTGTCCCGCT-3). The reaction was performed with an initial denaturation of 5 min at 94 °C followed by 30 cycles of 1 min at 94 °C, 1 min at 63 °C, and 1 min at 72 °C with a final extension at 72 °C for 7 min.

## Results

### *The promoter lesion of ChM-I was deacetylated by binding of HDAC2 in ChM-I-negative OS cell lines*

Three of seven OS cell lines (TAKAO, Saos2, and MG63) showed no expression of the ChM-I gene even in the RT-PCR analyses, among which two (TAKAO and Saos2) turned out to be positive on treatment with 5-Aza-dC (Fig. 1 A). The state of the histone tails of these seven OS cell lines was analyzed by Western blotting (Fig. 1B) and ChIP assay (Fig. 1C). The acetylation of global lesions of the histone H3 and H4 tails did not differ between the ChM-I-positive and negative cell lines (Fig. 1B). But the histone H3 and H4 tails associated with the lesion in the promoter of ChM-I was locally acetylated in ChM-I-positive cells, and deacetylated in the negative cells (Fig. 1C), indicating that the status of histone acetylation correlated with the expression of the ChM-I gene. To find the HDAC responsible for the deacetylation, the expression of HDAC2, HDAC3, and HDAC6 was analyzed by Western blotting, which showed no clear correlation with the expression of ChM-I gene (Fig. 1D). The ChIP assay, however, showed that HDAC2, but not HDA3 or HDAC6, bound to the promoter region in the ChM-I-negative cell lines (Fig. 1E). These results suggested that HDAC2 was

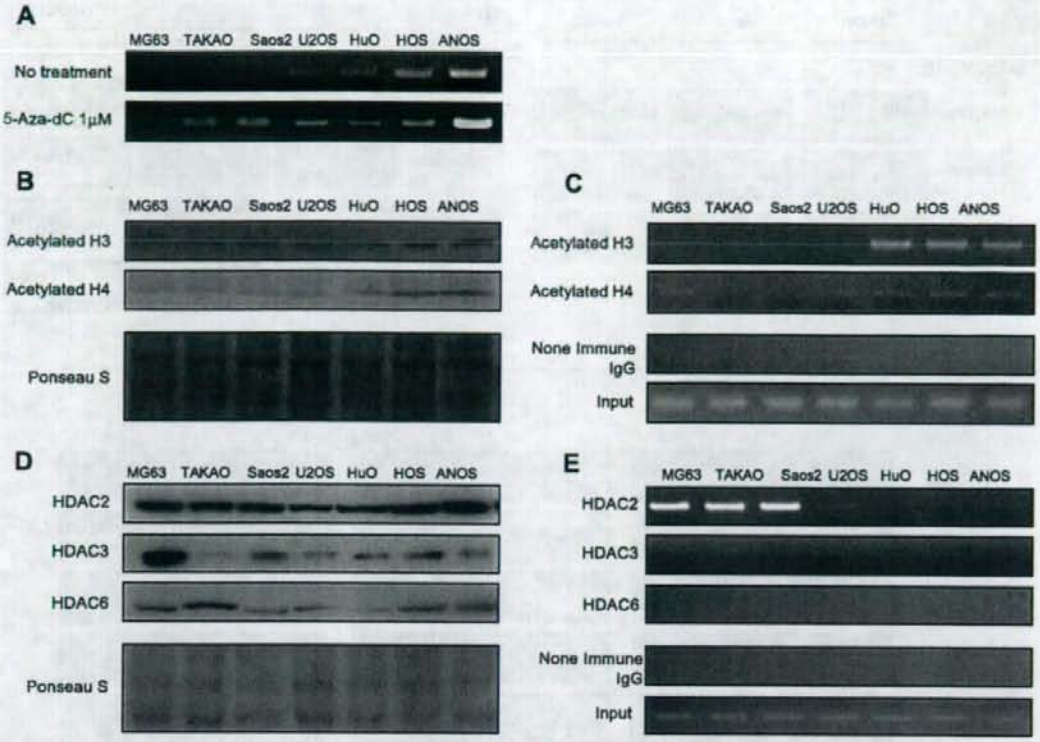


Fig. 1. Histone H3 and H4 tails surrounding the promoter of ChM-I were deacetylated by the binding of HDAC2 in ChM-I-negative OS cells. (A) mRNA expression of ChM-I before and after the treatment with 5-aza-dC (1 μM). (B) Protein expression of acetylated H3 and H4 tail in OS cells. (C) ChIP assay demonstrating the association of acetylated H3 and H4 with the core promoter region of the ChM-I gene in OS cells. (D) Protein expression of HDAC2, HDAC3, and HDAC6. (E) ChIP assay demonstrating the binding of HDACs to the core promoter region of the ChM-I gene in OS cells.

responsible for the deacetylation of histone associated with the promoter region of the ChM-I gene in ChM-I-negative OS cells.

### *Inhibition of HDAC2 restored the binding of Sp3 and the expression of ChM-I gene*

MS-275 is an inhibitor for class I HDACs including HDAC2. The global histone acetylation was promoted by MS-275 in both ChM-I-positive (ANOS) and negative (MG63 and TAKAO) cells (Fig. 2A), whereas the local histone acetylation status caused by the MS-275 treatment differed among the cell lines. Histone H4 was further acetylated in ANOS, and the acetylation of both histone H3 and H4 was induced in MG63. No such induction of histone acetylation was observed in TAKAO (Fig. 2B).

Then we analyzed the binding of Sp3 and HDAC2 to the promoter region of the ChM-I gene after the treatment with MS-275 and/or 5-Aza-dC (Fig. 2C). In ANOS, the binding status of Sp3 or HDAC2 was not changed by any treatment (Fig. 2C). In MG63, the binding of Sp3 was induced in association with the elimination of the binding of HDAC2 by MS-275, but not by 5-Aza-dC treatment (Fig. 2C). In TAKAO, the binding of Sp3 was induced by 5-Aza-dC treatment with no change in the binding of HDAC2, and treatment with MS-275 caused a reduction in the binding of HDAC2, but failed to induce the binding of Sp3 (Fig. 2C). Simultaneous treatment with 5-Aza-dC and MS-275 resulted in a reduction in the binding HDAC2. The expression of the ChM-I gene in three cell lines correlated with the status of Sp3 binding; MS-275 treatment and 5-Aza-dC treatment induced the expression in MG63 and TAKAO, respectively. The binding of Sp1, HDAC3, and HDAC6 was not changed by MS-275 and/or 5-aza-dC treatment in these three cell lines (Fig. 2C). We performed identical experiments using Saos2, another ChM-I-negative OS cell line, and obtained essentially the same results as in TAKAO (data not shown).

### *CpG methylation of the promoter lesion was demethylated by MS-275 in a DNA replication-dependent manner*

The induction of ChM-I gene expression in MG63 by HDACi was an unexpected result because the promoter

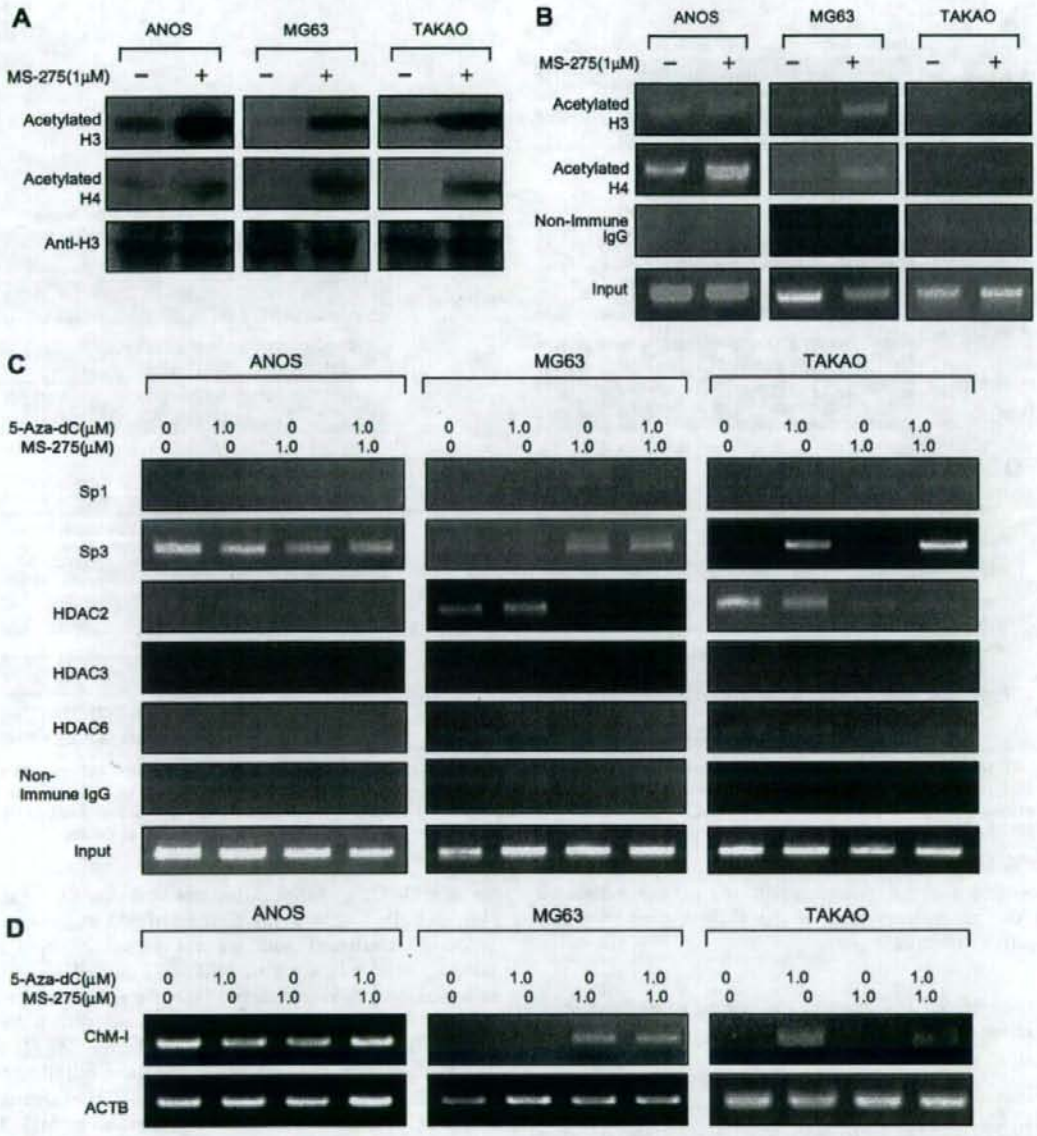


Fig. 2. Histone H3 and H4 tails were acetylated by MS-275, eliminating HDAC2. (A) Protein expression of acetylated H3 and H4 in OS cells with or without treatment with MS-275 (1 μM). (B) ChIP assay demonstrating the association of acetylated H3 and H4 with the core promoter region of the ChM-I gene in OS cells with or without treatment with MS-275 (1 μM). (C) ChIP assay demonstrating the binding of Sp1, Sp3, HDAC2, HDAC3, and HDAC6 with the core promoter region of the ChM-I gene in OS cells. Cells were treated with 5-Aza-dC and MS-275 at the indicated concentration. (D) mRNA expression of the ChM-I gene in OS cells treated with 5-Aza-dC and MS-275 at the indicated concentration.

region was heavily methylated in this cell line [1]. Bisulfite genomic sequencing of the promoter region revealed that the methylation of MG63 was significantly reduced and almost equivalent with that of ANOS (Fig. 3A). Methylation in the promoter region of TAKAO was also reduced but to much less of an extent (Fig. 3A). Conversion between acetylation and methylation of H3-K9 is known to regulate the methylation status of CpG [5]. Notably, the dimethylation of H3-K9 is known to be correlated with methylation of CpG [6]. Therefore, the modification of H3-

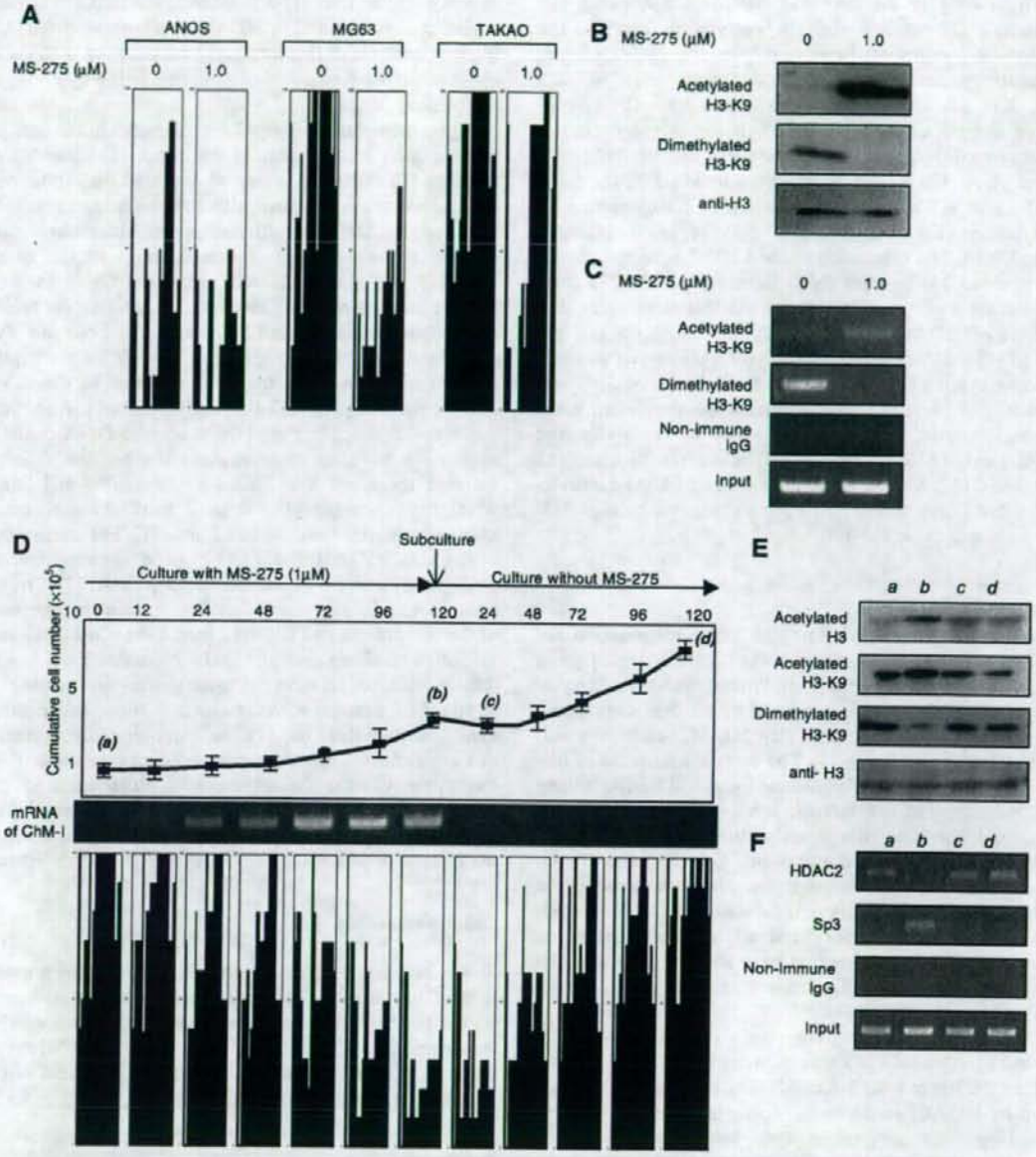


Fig. 3. Modification of the histone tail was associated with the methylation of CpG in the promoter region of the ChM-I gene. (A) Methylation status of the core promoter region of OS cells analyzed by bisulfite sequencing. Cells were treated with the indicated concentration of MS-275 for 96 h. *Y*-axis indicates the number of methylated alleles and *X*-axis indicates the position of each CpG site relative to the transcription start site. (B) Protein expression of acetylated H3-K9 and dimethylated H3-K9 in MG63 treated with the indicated concentration of MS-275. (C) ChIP assay demonstrating the association of acetylated H3-K9 and dimethylated H3-K9 with the core promoter region of ChM-I gene in MG63 cells treated with the indicated concentration of MS-275. (D) Temporal association of the mRNA expression and the methylation status of the core promoter region of the ChM-I gene in MG63 treated with MS275 (1 μM). Cumulative cell number (upper column), mRNA expression (middle column), and methylation status of the core promoter region of the ChM-I gene (lower column) were sequentially analyzed at the indicated time points. (E) Protein expression of acetylated H3, acetylated H3-K9, and dimethylated H3-K9 of MG63 at the time point indicated in (D). (F) ChIP assay demonstrating the binding of HDAC2 and Sp3 to the core promoter region of the ChM-I gene in MG63 at the time points indicated in (D).

K9 was analyzed by Western blotting (Fig. 3B) and ChIP assay (Fig. 3C). The dimethylation was converted to acetylation by MS-275 treatment in both global (Fig. 3B) and local promoter areas (Fig. 3C) in MG63.